

3D culture of HepaRG cells in GelMa and its application to bioprinting of a multicellular hepatic model

Marie Cuvellier, Frédéric Ezan, Hugo Oliveira, Sophie Rose, J.-C. Fricain, Sophie Langouët, Vincent Legagneux, Georges Baffet

▶ **To cite this version:**

Marie Cuvellier, Frédéric Ezan, Hugo Oliveira, Sophie Rose, J.-C. Fricain, et al.. 3D culture of HepaRG cells in GelMa and its application to bioprinting of a multicellular hepatic model. Biomaterials, 2021, 269, pp.120611. 10.1016/j.biomaterials.2020.120611 . hal-03095742

HAL Id: hal-03095742
https://hal.science/hal-03095742

Submitted on 25 Jan 2021

HAL is a multi-disciplinary open access archive for the deposit and dissemination of scientific research documents, whether they are published or not. The documents may come from teaching and research institutions in France or abroad, or from public or private research centers.

L'archive ouverte pluridisciplinaire **HAL**, est destinée au dépôt et à la diffusion de documents scientifiques de niveau recherche, publiés ou non, émanant des établissements d'enseignement et de recherche français ou étrangers, des laboratoires publics ou privés.

3D culture of HepaRG cells in GelMa and its application to bioprinting of a multicellular hepatic model

Cuvellier Marie[1], Ezan Frédéric[1], Oliveira Hugo[2,3], Rose Sophie[1], Fricain Jean-Christophe [2,3,4], Langouët Sophie[1], Legagneux Vincent[1], Baffet Georges[1]

[1]Univ Rennes, Inserm, EHESP, Irset (Institut de recherche en santé, environnement et travail) - UMR_S 1085, Rennes, France

[2] Université de Bordeaux, Bioingénierie tissulaire, 146, rue Léo Saignat, 33076 Bordeaux, France

[3] Inserm U1026, Bioingénierie tissulaire, 146, rue Léo Saignat, 33076 Bordeaux, France

[4] CHU Bordeaux, Services d'Odontologie et de Santé Buccale, F-33076 Bordeaux, France

marie.cuvellier@univ-rennes1.fr

Corresponding author : Georges Baffet, UMR 1085, IRSET, Inserm-University of Rennes 1, Campus de Villejean, CS 34317, 35043 Rennes, France. Tel: (33)2.23.23.45.92. E-mail: georges.baffet@inserm.fr

Authors declare no conflict of interest

Financial support : Supported by the Institut National de la Santé et de la Recherche Médicale (Inserm), University of Rennes 1, INCA #2018-142, Ligue contre le cancer du Grand Ouest. MC has been a recipient of a fellowship from Inserm and the Région Bretagne.

Authors contributions: CM: Investigation, Writing - original draft, review & editing; EF: Investigation; OH: Investigation, Resources, Writing - review & editing; RS: Resources, Methodology; FJC: Supervision; LS: Conceptualization; LV: Formal analysis, Writing - review & editing; BG, Conceptualization, Funding acquisition, Writing - original draft, review & editing

Journal Pre-proof

CRediT author statement

CM: Investigation, Writing - original draft, review & editing; EF: Investigation; OH: Investigation, Resources, Writing - review & editing; RS: Resources, Methodology; FJC: Supervision; LS: Conceptualization; LV: Formal analysis, Writing - review & editing; BG, Conceptualization, Funding acquisition, Writing - original draft, review & editing

Journal Pre-proof

Abstract:

Bioprinting is an emergent technology that has already demonstrated the capacity to create complex and/or vascularized multicellular structures with defined and organized architectures, in a reproducible and high throughput way. Here, we present the implementation of a complex liver model by the development of a three-dimensional extrusion bioprinting process, including parameters for matrix polymerization of methacrylated gelatin, using two hepatic cell lines, Huh7 and HepaRG. The printed structures exhibited long-term viability (28 days), proliferative ability, a relevant hepatocyte phenotype and functions equivalent to or better than those of their 2D counterparts using standard DMSO treatment. This work served as a basis for the bioprinting of complex multicellular models associating the hepatic parenchymal cells, HepaRG, with stellate cells (LX-2) and endothelial cells (HUVECs), able of colonizing the surface of the structure and thus recreating a pseudo endothelial barrier. When bioprinted in 3D monocultures, LX-2 expression was modulated by TGF-β-1 toward the induction of myofibroblastic genes such as ACTA2 and COL1A1. In 3D multicellular bioprinted structures comprising HepaRG, LX-2 and endothelial cells, we evidenced fibrillar collagen deposition, which is never observed in monocultures of either HepaRG or LX-2 alone. These observations indicate that a precise control of cellular communication is required to recapitulate key steps of fibrogenesis. Bioprinted 3D co-cultures therefore open up new perspectives in studying the molecular and cellular basis of fibrosis development and provide better access to potential inducers and inhibitors of collagen expression and deposition.

Keywords: Bioprinting, methacrylated gelatin, hepatocyte, HepaRG, 3D liver models

Abbreviations

2D: two-dimensions; 3D: three-dimensions; 3MC: 3-methylcholanthrene; CYP: Cytochromes P450; CDDP: cisplatine; DMSO: dimethyl sulfoxide; ECM: extracellular matrix; EdU: 5-ethynyl-2′-deoxyuridine; EROD: Ethoxyresorufin-O-deethylation GelMa: methacrylated gelatin; HSC: hepatic stellate cells; LAP: lithium phenyl-2,4,6 trimethylbenzoylphosphinate; MROD: Methyresorufin-O-deethylation; TGFβ-1: Transforming growth factor beta 1; TPEF: two-photon excitation microscopy; SHG second harmonic generation

Journal Pre-proof

Introduction:

The liver is the organ responsible for the biotransformation and elimination of drugs and xenobiotics. Therefore, developing *in vitro* assays based on human hepatic cells are one of the most critical steps for assessing the metabolism and/or toxicity of drugs or exogenous compounds (Stanley, 2017).

These last decades, conventional two-dimensional (2D) cell cultures of hepatic model systems have been extensively developed by many laboratories. However, murine and human normal hepatocytes do not survive more than one week in 2D culture and rapidly lose their differentiated functions (Elaut et al., 2006; LeCluyse et al., 1996) whereas transformed human hepatocytes derived from primary human hepatocytes do not, most of the time, recapitulate the differentiation status of native parenchymal cells (Gerets et al., 2012; Guo et al., 2011). Moreover, 2D cell culture of hepatic model systems does not reliably recapitulate the liver structure, phenotype and multicellular architecture, leading to a gap between observed *in vitro* toxicity and *in vivo* human hepatotoxicity (Berthiaume et al., 1996). Animal models have been the tool of choice for assessing the preclinical safety of new drug candidates and are still required by legislation. However, it is now recognized that the results obtained on animal models only partially recapitulate toxicity observed in humans and the specificities of the biotransformation of drugs have been largely described (Olson et al., 2000). Besides, ethical considerations related to the utilization of these models tend to limit their use.

To develop a physiological human liver model, the pharmaceutical industry is interested in developing an ideal *in vitro* model combining both the benefits of 2D and 3D cultures. Conventional 2D cultures, whether of primary, immortalized or stem cells derived hepatocytes, is still mainly used today during the first stage of biotransformation and hepatic toxicity studies. Easily usable, these controlled and standardized culture conditions make them good models for drug screening and to high-throughput testing. In recent decades, the 3D culture of hepatic cells has been able to overcome the weaknesses of 2D cultures providing, for example, a matrix environment that mimics the mechanical cues from hepatocyte microenvironment and promotes cell-cell interactions. (Bomo et al., 2016; Luebke-Wheeler et al., 2009; Proctor et al., 2017). 3D monoculture and co-culture of hepatic cells improve the viability and the functional capability of hepatocytes compared to 2D monolayer cultures.

The main prerequisite for developing an ideal 3D liver model is the ability to co-cultivate parenchymal and non-parenchymal cells as to mimic intercellular events and cross-talk (Bhandari et al., 2001; Loréal et al., 1993; Théret et al., 1997), and to mimic the complexity and diversity of metabolism and drug toxicity pathways (Khetani and Bhatia, 2007). The cells must remain viable and functional for several weeks in culture, which will allow studies long enough to reflect repeated low doses exposure as *in vivo*. The phenotype of the liver cellular model should be as close as possible to the *in vivo* phenotype, in particular the activity of phase I and II biotransformation enzymes and transporters, major actors in the metabolism of drugs. The model must be reproducible, robust and allow high throughput screening of the drug or compounds.

Journal Pre-proof

3D bioprinting offers an attractive alternative to classic 3D models (Murphy and Atala, 2014; Wang et al., 2007). The controlled and accurate cell deposition by the bioprinter provides 3D models with defined microarchitecture and the possibility to recreate vascularized structures (Bertassoni et al., 2014a; Grix et al., 2018). So far, very few efficient bioprinted hepatic models have been developed. In most of these models, long-term viability is not assured and few studies have evaluated the functionality of the printed cells or the toxicity and biotransformation of exogenous compounds (Billiet et al., 2014; Grix et al., 2018; Hiller et al., 2018; Ma et al., 2016). Bioprinting of murine hepatocytes has led to promising models in terms of long-term viability (Wang et al., 2006; Yan et al., 2005) but in addition to the ethical and commercial aspect, studies carried out on primary murine hepatocytes are limited by significant differences in metabolism and pharmacokinetics compared to human hepatocytes. One of the most successful and described bioprinted models was developed by the Organovo team. A primary human hepatocyte paste was co-printed with human stellate and HUVECs cells, fabricating a functional model of human liver tissue (Nguyen et al., 2016; Norona et al., 2016). Unfortunately, the cost and difficulty of obtaining freshly isolated primary cells, the inherent variability of human primary cell isolation and the use of homemade extrusion printers do not allow this model to be routinely replicated and to be applied to high throughput studies. We have developed here a cheap and easily usable 3D model using an Allevi commercial extruder. The selected ink, gelatin methacrylate (GelMa), is easily accessible or synthesizable and is widely used in extrusion-based systems (Kolesky et al., 2014; Loessner et al., 2016). We have optimized the printing conditions to obtain a good structural integrity as well as an optimal viability and cell differentiation over the long term.

The HepaRG cell line, isolated from hepatocarcinoma cells of a hepatitis B virus infected patient (Gripon et al., 2002), is currently the gold standard for transformed human hepatocytes. HepaRG cells retains bipotent hepatic progenitor-like characteristics and can partially recapitulate the liver phenotype when they are cultivated in the presence of DMSO at 1.7% to 2 % (v/v) in 2D (Aninat, 2005; Gripon et al., 2002; Guillouzo et al., 2007). 3D models of the HepaRG cell line have been showed to be an attractive tool for toxicological studies showing higher cell differentiation than in 2D culture (Lauschke et al., 2016; Leite et al., 2016). The HepaRG cell line, the “gold standard” for liver tests, and the LX-2 cell line, derived from activated human stellate cells (Xu, 2005), were successfully printed in a GelMa matrix to obtain a complex and functional 3D model. Not only the structures were shown to be viable for at least one month, but we have, for the first time, demonstrated the ability of the bioprinted HepaRG cells to differentiate and proliferate in a 3D environment in absence of DMSO.

The HepaRG cells were then used to mimic physiopathologicalogical phenomenon, hepatic fibrosis. *In vivo*, following chronic attacks, the secretion by hepatocytes and Kupffer cells of pro-fibrosing signals such as TGFβ-1 causes activation of quiescent hepatic stellate cells (HSC) which acquire a myofibroblastic phenotype. They become proliferating, contractile and activate tissue healing by

Journal Pre-proof

synthesizing components of the extracellular matrix (ECM) such as type I collagen. The *in vitro* study of mechanisms of development of hepatic fibrosis such as activation and matrix remodeling by stellate cells requires the establishment of cocultures between, inter alia, hepatic cells and hepatocytes (Loréal et al., 1993; Prestigiacomo et al., 2017, 2020; Théret et al., 1997). However, the culture of stellate cells remains today a technological obstacle in obtaining relevant hepatic fibrosis models. Primary HSCs, human or murine, are widely used but, when cultivated in a monolayer on rigid supports (such as plastic culture dishes), self-activate in 7 to 10 days from a quiescent to a myofibroblastic phenotype (Lim et al., 2002). We have demonstrated that, in our 3D system, LX-2 cells exhibit features of quiescent stellate cells and initiate an activation process in response to TGFβ-1 treatment. Moreover, we evidenced a deposition of fibrillar collagen when LX-2 cells were co-cultured with HepaRG and endothelial cells. These observations make our 3D system a promising model for liver fibrosis and open up new perspectives in studying the mechanisms of fibrogenesis, and the effects of exogenous factors on this process.

Journal Pre-proof

Material and Methods

Reagents

DMEM (41966-029) and William's E (22551-022) mediums were from Gibco (ThermoFisher, Waltham, MA USA). Lipofectamine RNAi max transfection reagent and TRIzol were from Invitrogen (Invitrogen, Carlsbad, CA, USA). Fetal bovine serum (FBS) and sucrose were purchased from Eurobio (Evry, France). Penicillin/ Streptomycin and FBS HyClone III were from Thermo Fisher (Waltham, MA USA), WST1 reagent, geneticin, Human insulin, hydrocortisone hemisuccinate, DMSO (D4540), formaldehyde, gelatin, 5-ethylnyl-2'-deoxyuridine, salicylamide, CY5-azide, ethoxyresorufin and methyresorufin, 3-methylcholanthrene (3MC) and rifampicine were from Sigma-Aldrich (St. Louis, MO, USA). Methacrylated gelatin (GelMa) was synthetized by the ART BioPrint (Bordeaux, FR). Lithium phenyl 2,4,6 trimethylbenzoylphosphinate (LAP) was from TCI (Japan) and U0126 was purchased from Promega (Mannheim, GE). Phenobarbital was from the Coopération pharmaceutique française. The Dapi Fluoromount-G was purchased from Southern Biotech (Birmingham, AL, USA). The EBM™-2 Endothelial Cell Growth basal medium and EGM™-2 BulletKit™ were from LONZA (Aubergenville, France).

Cell cultures

Huh7 cells (ECACC 01042712) were obtained from Health Protection Agency Culture Collections, Salisbury, UK. DNA transfections were carried out using Lipofectamine RNAi max transfection reagent according to the manufacturer's instructions. Briefly, cells were plated in a 35 mm-petri dish. 3 µL EmGFP-geneticin vector and 5 µL of Lipofectamine RNAi max were mixed in 200µL Opti-MEM® and then added to the cells. After overnight incubation, cells were incubated 24h in DMEM medium for 24h, then selected by geneticin treatment at 10mg.mL-1 during 48h. After selection, Huh7 GFP+ cells were cultured in DMEM containing 4.5g/L glucose and pyruvate supplemented with 10 % (v/v) FBS (EuroBio), 100 units.mL^{-1} penicillin and 100 µg.mL^{-1} streptomycin, 2 mM l-glutamine and 500 µg.mL^{-1} geneticin.

LX-2 were provided by Dr N. Theret (Irset, France) and were cultured in DMEM containing 4.5g/L glucose and pyruvate supplemented with 10 % (v/v) fetal bovine serum (EuroBio), 100 units.mL-1 penicillin, 100 µg.mL-1 streptomycin and 2 mM L-glutamine.

GFP-HUVECs (ZHC-2402, CellWorks, Buckingham, UK) were cultured in a mix of EBM™-2 Endothelial Cell Growth basal medium and William's E medium (1:1) supplemented with 10% (v/v) FBS Hyclone III, 100 units.mL^{-1} penicillin, 100 µg.mL-1 streptomycin, 5 µg.mL^{-1} human insulin, 2 mM L-glutamine, and 5 x 10^{-5} M hydrocortisone hemisuccinate. hFGF-B, VEGF, Ascorbic Acid, hEGF, GA-1000 and Heparin issued from the EGM™-2 BulletKit™ were added to the medium at concentrations recommended by the supplier.

Undifferentiated HepaRG cells (Biopredic, Saint Grégoire, France) were cultured in William's E medium without L-Glutamine supplemented with 10% (v/v) fetal bovine serum Hyclone III, 100 units.mL^{-1} penicillin, 100 µg.mL^{-1} streptomycin, 5 µg.mL^{-1} human insulin, 2 mM L-glutamine, and 5 x 10^{-5} M hydrocortisone hemisuccinate for 14 days. Hepatic differentiation in 2D culture was induced by treatment

Journal Pre-proof

with 2 % (v/v) DMSO for an additional 14 days. Undifferentiated HepaRG cells were cultivated on low attachment plate for 15h and the cluster of cells were harvested for mixing with GelMa before bio-printing (See patents n° EP2018030560320180516 / WO2019219828, INPI, National Institute of Industrial Property, France). Primary human hepatocytes (PHH) were obtained from the processing of biological samples through the Centre de Ressources Biologiques (CRB) Santé of Rennes BB-0033-00056. The research protocol was conducted under French legal guidelines and fulfilled the requirements of the local institutional ethics committee. PHH were isolated by a two-step collagenase perfusion procedure (Guguen-Guillouzo et al., 1982) and immediately proceeded.

Bio-Ink preparation and bioprinting

Methacrylated gelatin was synthesized as previously described (Kolesky et al., 2014). Briefly, a 10% (w/v) gelatin (Type A, 300 bloom from porcine skin, Sigma) solution, in PBS, was warmed at 60 °C for 2 h under stirring. Then, the temperature was set to 50 °C and 0.14 mL of methacrylic anhydride (Sigma) per gram of gelatin was added drop-wise. The solution was left to react for 4 hrs, under stirring, then diluted to 5% (w/v) in PBS. The reacted gelatin was precipitated using a 4-fold excess volume of cold acetone. The precipitated gelatin was recovered, vacuum dried for 30 minutes, and then redissolved at 10% (w/v) in PBS at 40 °C. It was then placed inside a 12–14 kDa molecular weight cutoff (MWCO) dialysis tubing (Sigma), aand dialyzed against deionized water for 3 days, with two daily water changes. The purified GelMa was frozen at -80 °C, freeze dried, and stored at -20 °C. Methacrylation degree was 60.4 ± 1.4 % (n=3), as determined by TNBS assay. GelMa was then dissolved in Williams'E medium at 37°C overnight. The bio-ink was then mixed to Lithium phenyl-2,4,6 trimethylbenzoylphosphinate dissolved in PBS (LAP, 10 mg.mL-1) and to the cells. The final cell-laden bio ink was composed of 5 % w/v GelMa, 0.3 or 0.1 % w/v LAP as indicated, 0.5 x 10^6/mL Huh7 or LX-2 cells or 2 x 10^6/mL undifferentiated HepaRG cells. The final cell-laden bio ink was composed of 5 % w/v GelMa, 0.3 or 0.1 % w/v LAP as indicated, 0.5 x 10^6/mL Huh7 or LX-2 cells or 2 x 10^6/mL undifferentiated HepaRG cells. The bioprinted structures for the study of HepaRG alone (Figure 3, 4, 5 and 6) have an estimated volume of 100 µL, encapsulating approximately 0.2x10^6 cells each. For the co-cultures (Figure 8), the bioprinted structure has a volume for HepaRG cells of approximately 150 µL (0.3x10^6 cells each) and LX-2 of 65 µL (0.0325x10^6 cells each); thus, giving a 10:1 cell ratio.

GelMa gels were characterized in terms of rheology. Briefly, photopolymerized gels, at 2.5, 5, 7.5 and 10 % (w/v) were soaked for 24 h in PBS and then loaded in a Kinexus pro$^+$ rheometer (Malvern Instruments, UK). Frequency sweeps were performed at a constant strain (0.1%) in an angular frequency range of 0.1–100 rad/s, at 37 °C.

For the bioprinting process, 100 µL of the bio-ink was cooled at 15°C and extruded through a 23G needle at 1.4 – 2.4 bar, at 480 mm/min, using the extrusion printer Allevi 2 (Allevi, Philadelphia, PA, USA) in 48 wells plate. The 3D construct was designed using the software OnShape (Cambridge, MA, USA). The printed constructs were exposed to violet light (405 nm, 7 mW/cm^2) during specified times to induce the radical polymerization of GelMa. They were then submerged in Williams' E medium with

Journal Pre-proof

supplements and incubated at 37°C and 5 % CO_2. For HUVECs seeding of constructs, the bioprinted HepaRG or HepaRG/LX-2 structures were cultured during a week, before being put in a low attachment plate containing a $1x10^6$/mL HUVECs suspension.

Cell viability

Cell viability assays were performed by using WST1 proliferation assay on cell-laden structures at the different days or times of culture. Briefly, structures were treated by 100 µl of WST1 reagent and put 30 min at 37°C. Absorbance was read at 440nm in a microplate reader (SpectrostarNano, BMG labtech, Champigny s/Marne, FR) and the values were converted into percentage of absorbance by comparison with controls at time 0. Measurement of LDH was performed on supernatants with the LDH-Glo™ Cytotoxicity Assay (Promega) by following manufacturer's instructions.

Proliferation quantification

For EdU incorporation, cell-laden constructs were treated 48h with EdU at 1 µM. For negative controls, cells were treated 24h prior EdU treatment by U126 at 20 µM until the fixation of the structures. Constructs were fixed and cryosectionned as described in the *Immunostaining procedure* section. EdU revelation was carried by performing permeabilization using 0.1 % (v/v) Triton X-100 for 10 min. Then, samples were treated with a mix of CuSO4 1(µM), Tris pH 8.5 (0.1 M), ascorbic acid (0.1M) and CY5-azide (1.5 µM, Sigma) for 1h. Cells were mounted with Dapi Fluoromount-G and the nucleus staining was monitored using a fluorescence microscope (Eclipse Ni-E, Nikon, Amsterdam, NL). Image processing was carried out using ImageJ software (http://imagej.nih.gov/ij/).

Immunostaining

Cell-laden structures were fixed in 4 % formaldehyde, washed 3x in PBS and stored at 4°C until use or immediately suspended in a 0.12M phosphate buffer containing 10 % w/v sucrose and incubated overnight. They were then embedded in a protective matrix composed of 7.5 % w/v gelatin and 10 % w/v sucrose, then frozen in isopentane and cryosectionned at a thickness of 7 µm. Slides were stained on the Discovery Automated IHC stainer using the discovery Rhodamin kit (Ventana Medical Systems, Tucson, AZ, USA). The concentrations and references of used primary antibodies can be found in Supplemental Table 1. After rinsing, signal enhancement was performed using the Ventana Rhodamin [1]kit and secondary antibody anti-rabbit HRP (760-4311, Roche) or secondary antibody anti-mouse HRP (760-4310, Roche) for 16 min of incubation. After removal of the instrument, slides were manually rinsed, stained when required with albumin antibody then a secondary antibody for albumin detection (Donkey anti goat 488), and mounted with Dapi Fluoromount-G.

RNA extraction and quantitative real time PCR

After 1, 2 or 4 weeks of culture, cell-laden structures were harvested, washed twice in PBS and total RNAs were extracted using TRIzol. The concentration of total RNAs were measured with a NanoDrop

Journal Pre-proof

ND-1000 (NanoDrop Technologies). cDNA were synthesized using the High Capacity cDNA reverse transcriptase kit (Applied Biosystems Foster City, CA, USA), and Real-time PCR was performed using the Power SYBR Green PCR master mix (Applied Biosystems Foster City, CA, USA). Primer-BLAST (NCBI USA), was used to design primer sequences which were purchased from Eurogentec (Searing, BE). All used primers are listed in Supplemental Table 2. The relative amount of measured mRNA in samples was determined using the $2^{-\Delta\Delta CT}$ method where $\Delta\Delta CT$ = (CTtarget – CT_{GAPDH}) sample- (CTtarget – CT_{GAPDH}) calibrator. Results were expressed as the n-fold difference of target gene expression in samples as compared with the mean expression values of the target gene. Figures 3B, 5C, 6B, S1C: target = HepaRG 2D DMSO; figures 7D, 7E: target = LX-2 2D; figure 8C, 8D: target = HepaRG 3D day 21, -TGFβ-1. All results are presented as mean ± SD of at least n=3 experiments.

Transcriptomic analysis

Total RNAs were purified from freshly isolated human hepatocytes (PHH T0) (n=5), of differentiated HepaRG after 14 days of culture on 2D (HRG 2D DMSO) (n=5) and at day 14 of culture on GelMa (HepaRG 3D GelMa) (n=4). The samples were concentrated using the RNA Clean & Concentrator-5 (Zymo, Irvine, CA, USA) and checked for RNA degradation based on the RNA Integrity Number (RIN>6). 3' sequencing RNA Profiling (3' SRP-seq) libraries were made at the GenoBIRD facility of Nantes, France, and sequenced using the HiSeq 2500 (Illumina, San Diego, CA, USA) following the described protocol (Soumillon et al., 2014). The analysis of the generated data was performed using R packages. The differentially expressed genes (FC > 2, $p < 0.05$) between HRG 2D DMSO and HRG GelMa D14 were functionally analyzed by computing enrichments for gene ontology (GO) terms, using the WEB-based database GEne SeT AnaLysis Toolkit (WebGestalT) restricted to protein coding data set. The presented data are selected as the top ten of the enriched categories, sorted by increasing enrichment ratios (FDR < 0.05).

Metabolic analysis

Cell culture medium samples were taken for the determination of albumin and urea content every 48h. Secreted albumin and pro-Col1a1 were quantified using the human serum albumin Duoset Enzyme Linked Immunosorbent Assay (ELISA) and the human pro-Col1a1 Duoset Enzyme Linked Immunosorbent Assay kits (R&D systems, Minneapolis, MN, USA), according to the manufacturer's instructions. Quantification was performed by measuring absorbance at 450 nm using a microplate reader (SpectrostarNano, BMG labtech, Champigny s/Marne, FR). Urea secretion in the medium was measured using a ChromaDazzle Urea Assay kit (AssayGenie, Dublin, IR) according to manufacturer's protocol, using medium as standard and reading the absorbance at 420nm (SpectrostarNano, BMG labtech, Champigny s/Marne, FR).

CYP activities measurement by fluorescence

After a 24H induction with DMSO 0.1 % v/v or 5 µM 3MC, Ethoxyresorufin-O-deethylation (EROD) was used as measurement of CYP1A activity and Methyresorufin-O-deethylation (MROD) for the CYP1A2

Journal Pre-proof

activity. EROD and MROD assays were performed as previously described (Burke and Mayer, 1983). The cells were washed with PBS and salicylamide (1.5 mM) was added to block phase II conjugation enzymes. 7-ethoxyresorufine or 7-methoxyresorufine was then added and the oxidation of the substrate was measured by fluorescent detection during 20 min, at 37°C (SpectraMax GeminiXS, Molecuar devices, San Jose, CA, USA). After the lecture, a WST1 test was performed to normalize activity with the quantity of viable cells.

CYP activities measurement by luminescence

Cytochrome P450 oxidase 2B6 and 3A4 activities were assessed by treating cells with DMSO 0.1 % (v/v), or activating them by phenobarbital (0.2 mM, 72h) (CYP2B6) or rifampicine (5 µM, 72h) (CYP3A4). Using the P450 GloAssay (Promega) according to the manufacturer's instructions, a CYP specific substrate Luciferin was added on cell-laden 3D constructs and incubated at 37 ˚C, 5% CO2, for 1 hour. Then, CYP-mediated conversion of Luciferin substrate to luciferin was determined. The supernatant was incubated with Luciferin detection reagent during 20 min at RT and the luminescence was measured. After the lecture, a WST1 test was performed to normalize activity with the quantity of viable cells.

SHG/TPEF microscopy

TPEF/SHG microscopy imaging was performed on mRIC facility of Biosit, University of Rennes1 (France). The SHG imaging system is composed of a confocal TCS SP5 scanning head (Leica Microsystems, Mannheim, Germany) mounted on a DMIRE2 inverted microscope (Leica Microsystems) and equipped with a MAITAI femtosecond laser (Spectra Physics, Santa Clara, CA). 60X water immersion objective (Olympus LUMFL 60W x 1.1NA) was used for applying an 820 nm excitation to the sample. The SHG signal was collected in the forward direction using the condenser (S1, NA ¼ 0.9 – 1.4; Leica Microsystems), and the TPEF was epi-collected in the backward direction. IRSP 715 bandpass and 410 nm infrared (IR) filters (10 nm full width at half-maximum, FWHM) were placed before the photomultiplier tube. The image processing was performed with ImageJ software (National Institutes of Health).

Statistical analysis

Unless clearly specified in caption, all variables are expressed as means ± standard deviations (SDs) of at least 3 experimentations with 3 technical replicates. Evaluation of the difference between the mean values in each group was performed using t-test or one-way analysis of variance (ANOVA) (GraphPad Prism 6, GraphPad Software, Inc.; La Jolla, CA, USA). Significant differences are represented for the following p-value thresholds: $p \leq 0.05$ (*/#); $p \leq 0.01$ (**/##); $p \leq 0.001$ (***), $p \leq 0.0001$ (****).

Journal Pre-proof

Results:

1. Physical properties of GelMa and Huh7 viability after bioprinting.

We first examined the polymerization and printability of various matrices that can be used for printing by an extrusion process (Supplemental Table 3). Three criteria were assessed for the selection of the matrix: 1/ its ability to polymerize and give a gel with sufficient rigidity to potentially maintain the structural and geometric integrity of the post-printing structures (polymerization) 2/ the polymerized gel had to be viscous enough to complete the extrusion process satisfactorily, with a regular filament shape during printing and maintaining the structure's architecture during printing (extrudability) 3/ the matrix should promote long-term culture of incorporated cells (cell culture). In view of our previous work on the incorporation and 3D culture of hepatic cells into collagen I matrix (Bomo et al., 2016), we tried to bioprint it, as well as methacrylated collagen (ColMa), by adding, or not, polymerizing adjuvants (Phytagel or carrageenan, two plant based gelling agents; methacrylated hyaluronic acid; collagen I) to compensate for their low viscosity. Unfortunately, none of these mixes made it possible to obtain sufficient viscosity to pass the 2nd criteria, i.e. the ability to form gels viscous enough to withstand the extrusion process.

We then turned to methacrylated gelatin, a matrix widely used in extrusion bioprinting due to its suitable mechanical properties and biocompatibility. Due to the thermo-induced gelling capacity of gelatin, GelMa (5% w/v) is able to polymerize at low temperature (15°C) to form a gel whose viscosity is sufficient to withstand the extrusion process (Criteria 1 and 3). To ensure optimal mechanical conditions of the GelMa promoting 3D hepatic cell culture, the physical properties of different GelMa compositions were analyzed. First, we examined the polymerization and printing properties of the gels as a function of the GelMa and LAP concentrations and different photopolymerization exposure times at 405 nm. At 20°C, a 2.5% concentration of GelMa was not sufficient to ensure polymerization and consequently an optimal viscosity for the printing process (figure 1A). A minimum concentration of LAP and an optimized time of light exposure have been defined to reduce the phototoxicity and the production of excess free radicals (Fairbanks et al., 2009) (figure 1B) while maintaining sufficient structural integrity of the printed GelMa for 28 days at 37 °C. Decreasing LAP concentration led to a diminished rate of cross-linking, and therefore to an altered structural integrity of the 3D bioprinted structures over time. Comparison of the weight of the gels obtained by polymerization in the presence of LAP concentrations at 0.1% or 0.3% showed a rapid decrease up to 40%, 5 hours after the polymerization process. Then, a constant weight for at least 28 days indicated good stability of the gel in the culture medium at 37°C (Figure 1C). As expected, rigidity, analyzed by rheology (Figure 1D), highly increased with the gelatin concentrations, consistent with other reports showing that the mechanical properties of the gelatin scaffolds were highly dependent on gel concentrations and cross-linking processes (Bertassoni et al., 2014b). A direct proportional relation was found between gelatin concentrations and the elastic (G') and viscous modulus (G") with an

Journal Pre-proof

exponential increased of G' from 0.05 to 2.12 kPa when the percentage of gelatin increased from 2.5 % to 15 %, respectively.

Next, we examined the short- and long-term viability of a hepatic transformed cell line, the Huh7 cells (Ni et al., 2019) in GelMa before and after bioprinting and cross-linking (GelMa 5%, LAP 0.1%, 1 min of light exposure). No decrease in Huh7 cell metabolism (WST1 activity) could be observed after 4 hours of bioprinting indicating that neither the GelMa, the cross-linking nor bioprinting processes were toxic at short times after seeding (figure 2A). Interestingly, for minimal LAP concentration (0.1%) and lighting times (1 min), the WST1 activity increased until day 14 and then remained constant thereafter at least until 28 days (figure 2B and 2C) showing that cells could survive and/or proliferate in the matrix after bioprinting. Furthermore, we showed that the cells were able to divide in GelMa since Ki67 positive cells could be detected at days 5 (12%), 10 (27%) and 14 (20%) (figure 2D), in accordance with the viability results described above (figure 2B and 2C). None or very few cleaved caspase-3 positive cells could be observed in these cultures 5, 10 and 14 days after seeding, whereas the cells responded well to an apoptotic inducer (CDDP) treatment at day 14 (figure 2D), indicating that cell death was very limited in these bioprinted structures. Based on these observations, we chose to work with GelMa and LAP concentrations of 5% (w/v) and 0.1% (w/v), respectively, and after 60 seconds of light exposure (at 405 nm).

2. Cluster organization, polarization and proliferation of HepaRG in GelMa

We applied this optimized bioprinting protocol to the gold standard human hepatic transformed cells, the HepaRG cell line. Undifferentiated HepaRG cells were either briefly (15h) cultivated in low-attachement plate in order to recreate partial cells-cells contact and bioprinted in a 5% GelMa, LAP 0.1% matrix, or left in 2D and fully differentiated by 2% DMSO (Figure 3A). In absence of these cells interactions enhancement, the HepaRG cells cannot fully differentiate in GelMa (data not showed). The 3D cultures were carried out in the absence of DMSO in order to avoid the non-specific induction of some CYP P450, i.e. the CYP3A4 and CYP2B6, which has been previously reported in DMSO-induced cultures of HepaRG (Aninat, 2005). HepaRG developed in small clusters of cells 7 days after seeding in the 3D GelMa hydrogel (Figure 3B). The cells appeared polarized as evidenced by the localization of E- and N-cadherins at the apico and lateral membranes. The hepatobiliary excretion transporter MRP2 located exclusively at apico/ canalicular areas, confirming the expected polarization of the cells in the clusters all over the culture time (Day 7, 14 and 28). The epithelial phenotype of these cells was assessed by measuring the expression of mesenchymal and epithelial markers. We found that *CDH2*/N-Cadherin (a mesenchymal marker) was less expressed in 3D hydrogels compared to 2D DMSO cultures while *CDH1*/E-Cadherin (an epithelial marker) and *ABCC2*/MRP2 (an hepatocyte marker), poorly expresses in undifferentiated 2D HepaRG (2D) were expressed at the same level in the two cultures.

Journal Pre-proof

Then, we evaluated the proliferation potential of the HepaRG cells in 3D by studying the expressions of cell division markers (Cyclin D1 and Ki67), as well as the incorporation of EdU, a readout of DNA replication. Only small differences in the kinetics of expressions of these proliferation markers could be observed (figure 3C). The late G1 and S phase markers, cyclin D1 and Ki67 respectively, were expressed in 10 to 20% of the cells, depending on the culture times. The same levels of EdU positive cells were detected in parallel to the Ki67 expression kinetic. The nuclear incorporation of EdU was largely abrogated by the MAP kinase inhibitor U0126, indicating that HepaRG proliferation in 3D was MEK1/2-ERK1/2 dependent (figure 3D).

3. Expression of differentiation and biotransformation markers.

To assess hepatic functions, we measured gene expressions by 3' SRP-RNA-Seq from RNAs HepaRG in 2D DMSO and in 3D GelMa culture at day 14 (Figure 4A). As expected, genes coding for regulatory pathways of cell structural organization such as cell-substrate, extracellular structure organization and cell-cell adhesion are clearly up-regulated, reflecting their adaptation to the microenvironment, whereas processes mainly linked to cell metabolism and catabolic process of endogen (peroxisomal transport, isoprenoid metabolic process, fatty acid metabolic/catabolic process) and exogen (drug catabolic process, small molecule catabolic process) compounds, were down regulated compared to 2D culture by DMSO.

Then, we looked at the liver-specific gene expressions (LiGEP signature) as defined by Kim *et al.*(Kim et al., 2017). This panel was based on the significantly differential RNA expressions between liver and non-liver samples. They developed an algorithm based on RNA-sequencing (RNA-seq) analysis to assess the differentiation or maturation status of 93 liver-specific genes validated by expression profiles in human Protein Atlas database and by quantitative real-time PCR analysis. A modified version of this original list, excluding, inter alia, genes from xenobiotic metabolism, was used for transcriptomic analyzes (Supplemental Table 4). We added RNAs from freshly isolated primary human hepatocyte (PHH T0), used here as a standard reference. The expression profile of freshly isolated primary human hepatocytes is considered to be closest to the liver *in vivo* but cannot be reproduced *in vitro* due to the extremely rapid dedifferention of the human hepatocytes in 2D. Here, if a decrease in the expression of hepatic genes can be observed during the comparison of hepaRG GelMa and HepaRG 2D DMSO with the freshly isolated PHH, one notes a maintenance of the expression of hepatic genes of the LiGEP signature with a great homology of the expression profiles of HepaRG in GelMa and 2D DMSO, with both HepaRG in 2D and 3D showing a quite similar pattern of many hepatic gene expression (*i.e. ALB, ALDOB, SERPINA1, FGA, FGB, FGG*…) (Figure 4B). By using real-time RT-qPCR, we confirmed that HepaRG cells in GelMa have a constant expression of various liver functions listed in the LiGEP heat map as well as receptors known to be involved in the biotransformation pathways of the drugs (*i.e. ALB, ALDOB, SERPINA1, HNF4A, NR1H4, NR1I2*), at short (7 days), medium (14 days) and long-term (28 days) after seeding (figure 5A). Their levels, throughout the 3D culture, were all superior to those of undifferentiated 2D HepaRG (2D) and were equal to or greater than those of cells in 2D DMSO conditions. We confirmed

Journal Pre-proof

these results by analyzing the secretions of albumin and urea (figure 5B and C), which remained constant during the whole culture process. Moreover, the low expressions of SOX9 and CK19 could indicate that the cells in the GelMa could preferentially differentiate towards a hepatic lineage rather than a biliary lineage, contrary to the 2D cultures were the two lineages coexist after DMSO treatment (figure 5D) (Aninat, 2005).

Concerning phase 1 biotransformation enzymes, the expression of these genes in 3D GelMa was closer to their expression in 2D DMSO than in PHH at T0 (figure 6A). By RT-qPCR, we validated that some mRNA expressions were equal (*CYP1A2*) or lower (*CYP3A4*, *CYP2B6*, *CYP2E1*, *CYP2C9*, *CYP2C19*) in 3D GelMa compared to 2D DMSO (figure 6B). In contrast, CYP1A and 1A2 activities could be induced in 3D cultures at the same level than in 2D DMSO (figure 6C). These induced activities can be observed all over the culture time allowing to analyze acute and chronic effects of the drugs in the 3D model until at least 28 days. CYP3A4, CYP2B6 and CYP1A2 activities could be induced by 2, 6, and 16-fold respectively indicating that 3D cells in GelMa respond well to all inducers (figures 6D and E). in the case of CYP2B6, activations were significativly higher in 3D than in the 2D DMSO cultures.
For phase 2 biotransformation enzymes and the transporters, as for phase 1 enzymes, the gene expression profiles in 3D GelMa were closer to those in 2D DMSO than in PHH T0 (supplemental figure 1A, 1B). As for the CYP mRNA expressions analyzed by RT-qPCR, expressions of the phase 2 enzymes and transporters were lower, equal to or greater in 3D compared to the 2D DMSO cultures, depending on the enzymes (supplemental figure 1C).

4. Evaluation of the fibrotic activity in micro engineered co-cultures.

Based on these encouraging observations about the viability and functionality of hepatocytes cultures in 3D GelMa, we used this matrix to build topologically controlled 3D cocultures of different liver cell types, in order to design a model for evaluating the fibrotic process *in vitro.* For this purpose, we first built bio-printed micro-engineered co-cultures using HepaRG, LX-2 (derived from activated stellate cells (Xu, 2005)) and HUVECS (derived from umbillical endothelial cells) cells that could allow to obtain a model for evaluating the fibrotic process *in vitro*.

As a preliminary step, we analyzed the survival of LX-2 cells cultured in the GelMa (Figure 7A). The WST1 activity remained stable or slightly increased during the first 14 days in the GelMa (figure 7B). Surprisingly, the LX-2 cells remained round in the matrix until at least 14 days of culture (figure 7C), whereas in collagen 1 matrix, they adopted a more elongated phenotype suggesting a transition to a myofibrobroblastic phenotype (Figure 7C). We then assessed the capacity of LX-2 cell to respond to TGFβ-1, a classical pro-fibrotic cytokine (Czaja et al., 1989). From day 2 of culture, cells were treated with vehicle (controls) or TGFß-1 (5 ng/mL every 48h) for two weeks (activation) or one week followed by an additional week without TGFß-1 (reversion) (Figure 7A). In GelMa, expression of *ACTA2*, the

Journal Pre-proof

major control of stellate cell activation, was clearly down regulated in control GelMa compared to cells cultivated on a 2D support (Figure 7D).

After TGFβ-1 treatment, the mRNA expressions of *ACTA2*, *COL1A1*, *MMP2* and *TIMP1*, encoding enzymes or components involved in ECM homeostasis, were clearly increased in a time-dependent manner (Figure 7E). These inductions were reversible and after TGFβ-1 removal at day 9, the mRNA expressions at day 16 were significantly decreased and return to a level equivalent to that observed in the untreated control.

Then, we compared bioprinted HepaRG alone and a co-culture of HepaRG and LX-2 (CoC), within a suitable structure with large channels allowing solute/gas exchanges with the medium (Figure 8A). HepaRG were bioprinted with large channels (Figure 8B, red design of left panel) and the LX-2 were bioprinted inside the channels (Figure 8B, blue) and, for both conditions, HUVECS cells were allowed to adhere and colonize the entire surface of the hydrogel. HepaRG cells without HUVECs neither LX2 were bioprinted as controls. Expression of the green fluorescent protein (GFP) allowed us to visualize the homogeneous seeding of fluorescent HUVECs cells at the surface of the gel, 4 days after seeding (Figure 8B, right panel). The albumin secretion of the CoC, compared to that of HepaRG + HUVECs, showed that albumin secretion kinetics over time was the same in the two conditions, indicating that the coculture did not alter or modify the high functionality of the HepaRG cells in the bioprinted GelMa (Supplemental Figure 2). Although a slight decrease in *ALB* gene expression is observed in the HepaRG + HUVECs and CoC conditions (Figure 8C), it can easily be explained by the presence, in these conditions, of non-hepatic RNA belonging to LX-2 or HUVECs cells.

After 14 days of culture, the three conditions (HepaRG, HepaRG+HUVECs, CoC) were activated or not by TGFβ-1 for 7 days (Figure 8A and B).When stimulated by TGFβ-1, a significant loss of hepatic functionality is reported by the fall in hepatic gene mRNA expression and albumin secretion (Figure 8C) and an increase of genes involved in ECM homeostasis (Supplemental Figure 3). Nevertheless, no specific release of LDH (a cell death marker) in the medium was observed (Figure 8C, right), and urea secretion remained stable over the 21 days of culture with or without TGFβ-1 treatment (Supplemental Figure 4). When analyzing *COL1A1* expression, we showed that basal expression is significantly higher in CoC than in HepaRG and HepaRG+HUVECs, at a level close to those of LX-2 in GelMa alone (Figure 8D, left). When activated by TGFβ-1, all conditions showed a significant increase in *COL1A1* expression. This gene expression is correlated to pro-collagen 1a1 secretion in medium (Figure 8D, right). Without TGFβ-1 stimulation, almost none pro-collagen 1a1 can be detected in HepaRG or HepaRG+HUVECs, whether TGFβ-1 treatment significatively induce its secretion. In CoC, a high basal secretion is measured at day 21 and no significant increase after TGFβ-1 activation can be detected. The level of pro-collagen 1a1 secretion in CoC is close to the one of TGFβ-1 activated HepaRG and HepaRG+HUVECs.

Journal Pre-proof

Our team has demonstrated the interest of second harmonic generation (SHG)/two-photon excitation microscopy (TPEF) as a tool to detect collagen fibrils *in vivo* and *in vitro* (Bomo et al., 2016; Gailhouste et al., 2010; Rouède et al., 2017). Briefly, SHG relies on the nonlinear optical interactions with non-centromeric fibrillar structures, such as collagen type I, allowing their detection and quantification in 3D tissues (Figure 8E, cyan). TPEF is based on the ability of a near infrared light to excite endogenous fluorophores in cells in thick samples (red). As a negative control, the GelMa alone did not give any SHG signal (data not shown). We used this technology to assess whether pro-collagen 1a1 was correlated to further collagen fibril formation. SHG microscopy was used to analyze the fibrillar collagen deposition in all conditions. Interestingly, SHG microscopy allowed to detect collagen fibrils within the matrix only in cocultures of CoC cells, stimulated or not by the TGFβ-1 (Figure 8E). We also confirmed that no collagen deposition could be observed in HepaRG cultured alone or with HUVECs, and, unexpectedly, activated or not by TGFβ-1. In such an interesting way, no collagen fibrils were ever observed after induction of the LX-2 cells by TGFβ-1 in our bioprinted GelMa model, when LX-2 cells were cultured alone.

Discussion

The main goal of this study was to bio-manufacture an adequate 3D cell/matrix model which could allow long-term differentiation of HepaRG cells and would serve as a base for further co-culture and microfluidic developments. Moreover, we have implemented an innovative technology to finely control the topology of these co-cultures. As a first step, we aimed to improve the 3D culture of the HepaRG cell line in GelMa, which promote cell-cell and cell-ECM interactions, characteristics that are essential for improving or maintaining cell functionality in the long term.

Very few studies, so far, have been able to develop an efficient and long-term viable 3D bioprinted hepatic model. One of the main obstacles is, among others, the long and critical process of bio-ink selection and determination of the parameters for its efficient use. Here, we used GelMa, a versatile and widely ink used in 3D bioprinting (Bertassoni et al., 2014b; Grix et al., 2018; Loessner et al., 2016), for the development of a 3D liver model based on the encapsulation of the HepaRG cell line. So far, the use of this bio-ink for the bioprinting of hepatocytes has been limited to 10% w/v GelMa matrices (Bertassoni et al., 2014b; Billiet et al., 2014; Grix et al., 2018) while we have chosen to decrease the concentrations up to 5% GelMa, the lowest concentration which showed bioprinting capacities (Figure 1). This choice was motivated by the fact that it has been previously well demonstrated that the decrease in matrix concentration, as well as its substitution rate, are correlated with a decrease in the stiffness of the gels (Billiet et al., 2014; Chen et al., 2012; Van Den Bulcke et al., 2000). The increasing mechanical stresses associated with this rigidity are known to negatively influence the proliferation and viability of the encapsulated cells. Likewise, the concentration of GelMa and its degree of crosslinking have been shown to be inversely proportional to the degree of porosity and to the size of the pores obtained (Chen et al., 2012). These pores, by ensuring the transport of nutrients and oxygen to the cells, are important actors in

Journal Pre-proof

the survival of the encapsulated cells. The formation of a network of large pores due to a reduced degree of methacrylation is also more permissive for the proliferation, the organization and the migration of the encapsulated cells (Chen et al., 2012). The LAP concentration, lighting duration and intensity has been shown to be proportionally linked to an increase in photo-induced crosslinking, and therefore in the stiffness of the gels (Van Den Bulcke et al., 2000). Here, by reducing it to the minimum usable (0.1%, 1 min, respectively), we considerably improved the viability of the cells over time, without losing structural stability of the printed structures. This also allowed us to improve cell viability by limiting exposition to free radicals produced during radical photopolymerization (Fairbanks et al., 2009) and by limiting the number of cross-linked methacrylate substitutes, thus allowing to finally tune the rigidity of 3D structures. These optimized parameters lead to a physical environment allowing us to achieve long term 3D cultures of bioprinted Huh7 and, for the first time, of the HepaRG cells line.

This culture, over a period of at least 28 days, of HepaRG cells is a major first step for obtaining bioprinted liver models competent for hepatotoxicity or ADME studies. Indeed, other existing bioprinted models are either based on the use of hepatic cell lines such as HepG2 or L02 (Bertassoni et al., 2014b; Billiet et al., 2014; Zhong et al., 2016), which are less metabolically competent and differentiated, or murine hepatic cells (Wang et al., 2006; Yan et al., 2005), which does not fully recapitulate human metabolism. HepaRG is a unique cell line which, due to its high metabolic capacities once fully differentiated in DMSO 2%, is currently the "gold standard" for xenobiotic metabolism and hepatotoxicity tests(Aninat, 2005; Anthérieu et al., 2012). So far, this cell line has been successfully printed in either GelMa (Grix et al., 2018) or a blend of ECM / Alginate / GelMa (Hiller et al., 2018) bio-inks. In these previous models, the cells are, at best, viable over 14 days, a time too short to study chronic treatment toxicity, a main limitation for chronic toxicity evaluation assays. Here, we could demonstrate continuous viability for at least 4 weeks. Also, in our 3D model, cells self-organize into polarized structures, mimicking the hepatocyte polarization in-vivo, as shown by the specific location of E Cadherin and MRP2. The establishment of a cell architecture that recapitulates E-Cadherin-dependent interactions is probably one of the factors for the maintenance of long term hepatic functionality in our models, as E-Cadherin is known to inhibit *in vivo* signaling pathways inducing hepatocyte dedifferentiation (Nagaoka et al., 2002; Vinken et al., 2006). We assume that the re-creation of these cell-cell interactions is due, as in many 3D hepatic models (Bomo et al., 2016; Luebke-Wheeler et al., 2009), to their culture in a 3D matrix environment whose stiffness is closer to that of a healthy liver (± 4.5 kPa), as compared to 2D cultures on plastic plates (~ $1x10^7$ kPa) (Discher et al., 2005). Furthermore, early interactions between cells are also critical for the long-term differentiation of the HepaRG cells in GelMa. Indeed, HepaRG must be seeded transiently on low attachment plate before being embedded into the Gel-MA matrix. In absence of these early cell interactions enhancement, the HepaRG cannot fully differentiated in GelMa (data not shown).

The HepaRG cell line shows great plasticity in 2D culture, being able to differentiate to both biliary- and hepatocyte-like cells (Cerec et al., 2019). After seeding at low density, the cells actively proliferate until they reach confluency and differentiate toward these two lineages. A maximum of differentiation is

Journal Pre-proof

reached after 2 weeks exposure to DMSO, and hepatocyte-like cells represent at least 50 % of the cell population. Our data on HepaRG cells in GelMa, cultivated without DMSO showed survival and hepatic differentiation close or higher to the cells cultured in 2D with DMSO. The differentiation was optimal at 14 days of culture and stayed at a high level for up to 28 days. Noteworthy, HepaRG bioprinted in GelMa seemed to differentiate preferentially toward a hepatic lineage, although the exact phenotype must be refined by extended analysis of immunohistochemical and transcriptomic profiles. This observation is in line with previous studies showing that HepaRG cells encapsulated in 3D matrices form hepatocyte-like colonies rather than cholangiocytes (Higuchi et al., 2019; Rebelo et al., 2015).

A major interest of developing 3D hepatic models is to use them as an *in vitro* alternative to screen the hepatotoxicity and xenobiotics metabolism. This implies that the metabolic capacities of these models must be as close as possible to those observed *in vivo*. However, with the exception of the ExVive 3D model (Nguyen et al., 2016; Norona et al., 2016), few bio-printed liver models have been evaluated based on these capacities. Bioprinted structures based on HepaRG cultures are constrained by the need to cultivate those cells for 2 weeks in DMSO to reach optimal differentiation, removal of DMSO from the medium resulting in a quick fall in hepatic differentiation markers (Aninat, 2005). This is why actual HepaRG bioprinted models are based, so far, on the encapsulation of DMSO pre-differentiated cells on the matrix before bioprinting (Grix et al., 2018; Hiller et al., 2018; Yang et al., 2020). Moreover, the quantification of the metabolic capacities of the models are limited, based solely on the evaluation of the expression or activity of the sole CYP3A4, without a significant improvement in metabolic activities compared to cells in 2D (Hiller et al., 2018). Thus, their use as hepatic models for xenobiotic metabolism has so far been extremely limited. In an interesting way, 3D cultured hepatocytes in GelMa were able to differentiate in the absence of DMSO. We showed a nearly equivalent expression of the biotransformation enzymes of phase 1 as compared to the 2D DMSO cultures, although their activities (CYP1A, 1A2, 2B6, 3A4) could be induced throughout the 3D culture at a higher rate. We thus demonstrate, compared to pre-existing models, the capacity of bioprinted HepaRG in GelMa to ensure, in the short, medium and long term (7, 14 and 28 days of culture), the biotransformation of xenobiotics at levels equal to or greater than fully 2D differentiated cells. This will allow to study the effects of chronic exposure to drugs and environmental products, in the absence of DMSO, which is a powerful reactive oxygen species producer and inductor of numerous CYPs, including the CYP3A4 and CYP2B6.

Another strength of our model, never demonstrated so far, is the ability of the differentiated HepaRG cells to constantly proliferate throughout the culture in GelMa. Thus, 3D cultures of HepaRG in GelMa overcome a major limitation of 2D cultures where proliferation and differentiation are mutually exclusive. These proliferative and differentiated properties of the HepaRG cells will be of great interest for studies focusing on the genotoxicity induced by drugs and environmental contaminants that need to be metabolized by the liver to produce genotoxic and/or mutagenic products (Langouët et al., 2001).

Journal Pre-proof

Models where different liver cell types are co-cultured in 3D partially recreate the complex interactions between parenchymal and non-parenchymal cells, allowing to explore physiological pathways in a context closer to that of *in vivo* organs (Leite et al., 2016; Messner et al., 2013; Prestigiacomo et al., 2017, 2020). We demonstrated that the bioprinted co-culture of HepaRG / LX-2 / HUVECS in GelMa constitutes a suitable model for studying collagen synthesis and deposition, emphasizing the major role of regulation between parenchymal and non-parenchymal cells in the collagen deposition (Loréal et al., 1993). This might be a major advance for studying hepatic fibrosis, as there are currently few *in vitro* physiological models of this pathology. Indeed, such models have to deal with several constraints, among them the need of putting together different cell types involved in hepatic fibrosis, the ability of stellate cells to activate towards a myofibroblastic phenotype, and a 3D environment allowing the ensuing progressive deposition of the ECM (van Grunsven, 2017; Leite et al., 2016; Norona et al., 2016). The reaction of HepaRG cells to TGFβ-1, whether in mono or co-culture, could mimic that found in the progressive development of fibrosis *in vivo*. Indeed, during this pathology, the TGFβ-1 released by the activated stellate cells is a promoter of fibroblastic/migratory phenotype. *In vitro*, the dedifferentiation of human hepatocytes was also objectified by the decrease of the expression of *ALB* and *HNF4A* after TGFβ-1 treatment (Caja et al., 2011). For the stellate cells model, we present, as already described by Norona et al., the maintenance for several weeks, of the LX-2 cell line (a cell line obtained from activated human primary stellate cells), in a "quiescent"-like phenotype. Unlike LX-2 cultured in 2D, the expression and synthesis of two markers of the activated HSC phenotype, respectively *ACTA2* and type I collagen, are strongly inhibited when the cells are embedded in a GelMa matrix, confirming the capacity of a flexible matrix to support the quiescence of stellate cells *in vitro* (Norona et al., 2016; Prestigiacomo et al., 2020; Sohara et al., 2002). As *in vivo*, the LX-2 cells remain however capable to respond to pro-fibrosing molecules such as TGFß-1, and, strikingly, to reverse to a "quiescent"-like phenotype upon withdrawn of this pro-fibrotic cytokine. It must be noted that the reversibility of this activation, as seen in our model, is also described *in vivo* (Kisseleva et al., 2012; Troeger et al., 2012), and in *in vitro* murine models (Prestigiacomo et al., 2020) but has yet to be precisely described in an *in vitro* human model (Sohara et al., 2002). LX-2 cells cultured in GelMa thus offer new perspectives for the study of cellular mechanisms linked to the activation and reversion of HSCs, in the context of human hepatic fibrosis progression and reversion.

Here, we show that activation by TGFβ-1 of HepaRG, HepaRG + HUVECs, LX-2 and CoC cells strongly induces the expression of the COL1A1 gene, and the secretion by these cells of pro-collagen1a1. Noteworthy, although the use of SHG biphotonic microscopy did not evidence any deposit in presence of TGFβ-1 of collagen fibers, a major marker of the development of hepatic fibrosis, in monocultures of LX-2, HepaRG, HepaRG + HUVECs cells. This deposit was detectable only in co-culture with HepaRG, LX-2 and endothelial cells even in absence of TGFβ-1. This illustrates and confirms the fact that the development of fibrosis is a complex phenomenon, strongly based on cell communication between the different cell types. Thus, the *in vitro* secretion of matrix proteins such as pro-collagen Ia1, as well as the synthesis of matrix remodeling factors, which can be detected in vitro in 2D mono-cultures of hepatocytes

Journal Pre-proof

(Hatahara and Seyer, 1982) or HSCs, might not be translated by a further organization in fibrillar structure, thus lacking a critical step for mimicking in vivo liver micro-environment.

The article presented here focuses on determining the parameters for using a 3D bioprinting matrix, the GelMa, which allows 3 things: 1/ physico-mechanical parameters allowing it to be used in 3D bioprinting, as shown by the impression of two different models, in mono and coculture, 2 / the DMSO-free differentiation, in this matrix, of HepaRG cells towards a hepatic phenotype by the microenvironment 3 / the maintenance of stellate cells, here LX -2, at a quiescent stage that can be activated thanks to these same conditions. The results obtained in our study confirm the importance of sophisticated interactions between the different hepatic cell types to obtain a deposit of collagen and to build relevant pathological models. This further illustrates the need for developing topologically controlled 3D co-culture models to recapitulate the progression and reversion of liver fibrosis. Future studies will expand the genomic and histologic characteristics of these bioprinted fibrosis models in the presence of pro- and anti-fibrotic drugs. Finally, coupling bioprinting techniques with perfusion-enabled channel systems combining HepaRG and human stellate cells will be developed in the future to improve organ-on-chip applications for pharmaceutical developments. Likewise, the use of 3D bioprinting, under our conditions, for the creation of chips coupled with microfluidic systems seem to us to be promising options.

Journal Pre-proof

Acknowledgements

The authors thank the Dr Nathalie Theret (IRSET) for giving us the LX-2 cell line and the platforms from the SFR Biosit (UMS CNRS 3480 / US INSERM 018, Biogenouest, University of Rennes 1): Microfluidic & Bioprinting Facility of Biosit, MRic-Photonics, MRic-Biphoton, H_2P_2, CRB Santé of Rennes.

Bibliography

Aninat, C. (2005). Expression of cytochromes p450, conjugating enzymes and nuclear receptors in human hepatoma HepaRG cells. Drug Metab. Dispos. *34*, 75–83.
Anthérieu, S., Chesné, C., Li, R., Guguen-Guillouzo, C., and Guillouzo, A. (2012). Optimization of the HepaRG cell model for drug metabolism and toxicity studies. Toxicol. In Vitro *26*, 1278–1285.
Bertassoni, L.E., Cecconi, M., Manoharan, V., Nikkhah, M., Hjortnaes, J., Cristino, A.L., Barabaschi, G., Demarchi, D., Dokmeci, M.R., Yang, Y., et al. (2014a). Hydrogel bioprinted microchannel networks for vascularization of tissue engineering constructs. Lab. Chip *14*, 2202–2211.
Bertassoni, L.E., Cardoso, J.C., Manoharan, V., Cristino, A.L., Bhise, N.S., Araujo, W.A., Zorlutuna, P., Vrana, N.E., Ghaemmaghami, A.M., Dokmeci, M.R., et al. (2014b). Direct-write bioprinting of cell-laden methacrylated gelatin hydrogels. Biofabrication *6*, 024105.
Berthiaume, F., Moghe, P.V., Toner, M., and Yarmush, M.L. (1996). Effect of extracellular matrix topology on cell structure, function, and physiological responsiveness: hepatocytes cultured in a sandwich configuration. FASEB J. *10*, 1471–1484.
Bhandari, R.N.B., Riccalton, L.A., Lewis, A.L., Fry, J.R., Hammond, A.H., Tendler, S.J.B., and Shakesheff, K.M. (2001). Liver Tissue Engineering: A Role for Co-culture Systems in Modifying Hepatocyte Function and Viability. Tissue Eng. *7*, 345–357.
Billiet, T., Gevaert, E., De Schryver, T., Cornelissen, M., and Dubruel, P. (2014). The 3D printing of gelatin methacrylamide cell-laden tissue-engineered constructs with high cell viability. Biomaterials *35*,

49–62.
Bomo, J., Ezan, F., Tiaho, F., Bellamri, M., Langouët, S., Theret, N., and Baffet, G. (2016). Increasing 3D Matrix Rigidity Strengthens Proliferation and Spheroid Development of Human Liver Cells in a Constant Growth Factor Environment. J Cell Biochem *117*, 708–720.
Burke, M.D., and Mayer, R.T. (1983). Differential effects of phenobarbitone and 3-methylcholanthrene induction on the hepatic microsomal metabolism and cytochrome P-450-binding of phenoxazone and a homologous series of its n-alkyl ethers (alkoxyresorufins). Chem. Biol. Interact. *45*, 243–258.
Caja, L., Bertran, E., Campbell, J., Fausto, N., and Fabregat, I. (2011). The transforming growth factor-beta (TGF-β) mediates acquisition of a mesenchymal stem cell-like phenotype in human liver cells. J. Cell. Physiol. *226*, 1214–1223.
Cerec, V., Glaise, D., Garnier, D., Morosan, S., Turlin, B., Drenou, B., Gripon, P., Kremsdorf, D., Guguen-Guillouzo, C., and Corlu, A. (2019). Transdifferentiation of hepatocyte-like cells from the human hepatoma HepaRG cell line through bipotent progenitor. Hepatology *45*, 957–967.
Chen, Y.-C., Lin, R.-Z., Qi, H., Yang, Y., Bae, H., Melero-Martin, J.M., and Khademhosseini, A. (2012). Functional Human Vascular Network Generated in Photocrosslinkable Gelatin Methacrylate Hydrogels. Adv. Funct. Mater. *22*, 2027–2039.
Czaja, M.J., Weiner, F.R., Flanders, K.C., Giambrone, M.A., Wind, R., Biempica, L., and Zern, M.A. (1989). In vitro and in vivo association of transforming growth factor-beta 1 with hepatic fibrosis. J Cell Biol 2477--2482.
Discher, D.E., Janmey, P., and Wang, Y. (2005). Tissue cells feel and respond to the stiffness of their substrate. Science *310*, 1139–1143.
Elaut, G., Henkens, T., Papeleu, P., Snykers, S., Vinken, M., Vanhaecke, T., and Rogiers, V. (2006). Molecular Mechanisms Underlying the Dedifferentiation Process of Isolated Hepatocytes and Their Cultures. Curr. Drug Metab. *7*, 629–660.
Fairbanks, B.D., Schwartz, M.P., Bowman, C.N., and Anseth, K.S. (2009). Photoinitiated polymerization of PEG-diacrylate with lithium phenyl-2,4,6-trimethylbenzoylphosphinate: polymerization rate and cytocompatibility. Biomaterials *30*, 6702–6707.
Gailhouste, L., Grand, Y.L., Odin, C., Guyader, D., Turlin, B., Ezan, F., Désille, Y., Guilbert, T., Bessard, A., Frémin, C., et al. (2010). Fibrillar collagen scoring by second harmonic microscopy: A new tool in the assessment of liver fibrosis. J. Hepatol. *52*, 398–406.
Gerets, H.H.J., Tilmant, K., Gerin, B., Chanteux, H., Depelchin, B.O., Dhalluin, S., and Atienzar, F.A. (2012). Characterization of primary human hepatocytes, HepG2 cells, and HepaRG cells at the mRNA level and CYP activity in response to inducers and their predictivity for the detection of human hepatotoxins. Cell Biol. Toxicol. *28*, 69–87.
Gripon, P., Rumin, S., Urban, S., Le Seyec, J., Glaise, D., Cannie, I., Guyomard, C., Lucas, J., Trepo, C., and Guguen-Guillouzo, C. (2002). Infection of a human hepatoma cell line by hepatitis B virus. Proc. Natl. Acad. Sci. *99*, 15655–15660.
Grix, T., Ruppelt, A., Thomas, A., Amler, A.-K., Noichl, B., Lauster, R., and Kloke, L. (2018). Bioprinting Perfusion-Enabled Liver Equivalents for Advanced Organ-on-a-Chip Applications. Genes *9*, 176.
van Grunsven, L.A. (2017). 3D in vitro models of liver fibrosis. Adv. Drug Deliv. Rev. *121*, 133–146.
Guguen-Guillouzo, C., Campion, J.P., Brissot, P., Glaise, D., Launois, B., Bourel, M., and Guillouzo, A. (1982). High yield preparation of isolated human adult hepatocytes by enzymatic perfusion of the liver. Cell Biol. Int. Rep. *6*, 625–628.
Guillouzo, A., Corlu, A., Aninat, C., Glaise, D., Morel, F., and Guguen-Guillouzo, C. (2007). The human hepatoma HepaRG cells: A highly differentiated model for studies of liver metabolism and toxicity of xenobiotics. Chem. Biol. Interact. *168*, 66–73.
Guo, L., Dial, S., Shi, L., Branham, W., Liu, J., Fang, J.-L., Green, B., Deng, H., Kaput, J., and Ning, B. (2011). Similarities and differences in the expression of drug-metabolizing enzymes between human hepatic cell lines and primary human hepatocytes. Drug Metab. Dispos. Biol. Fate Chem. *39*, 528–538.
Hatahara, T., and Seyer, J.M. (1982). Procollagen production by rat hepatocytes in primary culture. Biochim. Biophys. Acta BBA - Gen. Subj. *716*, 431–438.
Higuchi, Y., Kawai, K., Kanaki, T., Yamazaki, H., Chesné, C., Guguen-Guillouzo, C., and Suemizu, H. (2019). Functional polymer-dependent 3D culture accelerates the differentiation of HepaRG cells into mature hepatocytes. Hepatol. Res. *46*, 1045–1057.
Hiller, T., Berg, J., Elomaa, L., Röhrs, V., Ullah, I., Schaar, K., Dietrich, A.-C., Al-Zeer, M., Kurtz, A., Hocke, A., et al. (2018). Generation of a 3D Liver Model Comprising Human Extracellular Matrix in an

Journal Pre-proof

Alginate/Gelatin-Based Bioink by Extrusion Bioprinting for Infection and Transduction Studies. Int. J. Mol. Sci. *19*, 3129.
Ho, M.T., Kim, Y.M., Yu, D.-Y., Lee, D.H., Cho, M., and Hyun, C. (2014). TGF-β secreted from activated hepatic stellate cells may induce the transdifferentiation of hepatocytes into hepatocarcinoma in HBx-expressing livers. J. Korean Soc. Appl. Biol. Chem. *57*, 529–538.
Khetani, S.R., and Bhatia, S.N. (2007). Microscale culture of human liver cells for drug development. Nat. Biotechnol. *26*, 120–126.
Kim, D.-S., Ryu, J.-W., Son, M.-Y., Oh, J.-H., Chung, K.-S., Lee, S., Lee, J.-J., Ahn, J.-H., Min, J.-S., and Ahn, J. (2017). A liver-specific gene expression panel predicts the differentiation status of in vitro hepatocyte models. Hepatology *66*, 1662–1674.
Kisseleva, T., Cong, M., Paik, Y., Scholten, D., Jiang, C., Benner, C., Iwaisako, K., Moore-Morris, T., Scott, B., Tsukamoto, H., et al. (2012). Myofibroblasts revert to an inactive phenotype during regression of liver fibrosis. Proc. Natl. Acad. Sci. *109*, 9448–9453.
Kolesky, D.B., Truby, R.L., Gladman, A.S., Busbee, T.A., Homan, K.A., and Lewis, J.A. (2014). 3D Bioprinting of Vascularized, Heterogeneous Cell-Laden Tissue Constructs. Adv. Mater. *26*, 3124–3130.
Langouët, S., Welti, D.H., Kerriguy, N., Fay, L.B., Huynh-Ba, T., Markovic, J., Guengerich, F.P., Guillouzo, A., and Turesky, R.J. (2001). Metabolism of 2-Amino-3,8-dimethylimidazo$[$4,5-f$]$-quinoxaline in Human Hepatocytes: 2-Amino-3-methylimidazo$[$4,5-f$]$quinoxaline-8-carboxylic Acid Is a Major Detoxication Pathway Catalyzed by Cytochrome P450 1A2. Chem. Res. Toxicol. *14*, 211–221.
Lauschke, V.M., Hendriks, D.F.G., Bell, C.C., Andersson, T.B., and Ingelman-Sundberg, M. (2016). Novel 3D Culture Systems for Studies of Human Liver Function and Assessments of the Hepatotoxicity of Drugs and Drug Candidates. Chem Res Toxicol.
LeCluyse, E.L., Bullock, P.L., and Parkinson, A. (1996). Strategies for restoration and maintenance of normal hepatic structure and function in long-term cultures of rat hepatocytes. Adv. Drug Deliv. Rev. *22*, 133–186.
Leite, S.B., Roosens, T., El Taghdouini, A., Mannaerts, I., Smout, A.J., Najimi, M., Sokal, E., Noor, F., Chesne, C., and van Grunsven, L.A. (2016). Novel human hepatic organoid model enables testing of drug-induced liver fibrosis in vitro. Biomaterials *78*, 1–10.
Lim, Y.S., Kim, K.-A., Jung, J.-O., Yoon, J.-H., Suh, K.-S., Kim, C.Y., and Lee, H.J. (2002). Modulation of cytokeratin expression during in vitro cultivation of human hepatic stellate cells: evidence of transdifferentiation from epithelial to mesenchymal phenotype. Histochem. Cell Biol. *118*, 127–136.
Loessner, D., Meinert, C., Kaemmerer, E., Martine, L.C., Yue, K., Levett, P.A., Klein, T.J., Melchels, F.P.W., Khademhosseini, A., and Hutmacher, D.W. (2016). Functionalization, preparation and use of cell-laden gelatin methacryloyl–based hydrogels as modular tissue culture platforms. Nat. Protoc. *11*, 727–746.
Loréal, O., Levavasseur, F., Fromaget, C., Gros, D., Guillouzo, A., and Clément, B. (1993). Cooperation of Ito cells and hepatocytes in the deposition of an extracellular matrix in vitro. Am. J. Pathol. *143*, 538–544.
Luebke-Wheeler, J.L., Nedredal, G., Yee, L., Amiot, B.P., and Nyberg, S.L. (2009). E-Cadherin protects primary hepatocyte spheroids from cell death by a caspase-independent mechanism. Cell Transplant. *18*, 1281–1287.
Ma, X., Qu, X., Zhu, W., Li, Y.-S., Yuan, S., Zhang, H., Liu, J., Wang, P., Lai, C.S.E., Zanella, F., et al. (2016). Deterministically patterned biomimetic human iPSC-derived hepatic model via rapid 3D bioprinting. Proc. Natl. Acad. Sci. *113*, 2206–2211.
Messner, S., Agarkova, I., Moritz, W., and Kelm, J.M. (2013). Multi-cell type human liver microtissues for hepatotoxicity testing. Arch. Toxicol. *87*, 209–213.
Murphy, S.V., and Atala, A. (2014). 3D bioprinting of tissues and organs. Nat. Biotechnol. *32*, 773–785.
Nagaoka, M., Ise, H., and Akaike, T. (2002). Immobilized E-Cadherin model can enhance cell attachment and differentiation of primary hepatocytes but not proliferation. Biotechnol. Lett. *24*, 1857–1862.
Nguyen, D.G., Funk, J., Robbins, J.B., Crogan-Grundy, C., Presnell, S.C., Singer, T., and Roth, A.B. (2016). Bioprinted 3D Primary Liver Tissues Allow Assessment of Organ-Level Response to Clinical Drug Induced Toxicity In Vitro. PLoS ONE *11*, e0158674.
Norona, L.M., Nguyen, D.G., Gerber, D.A., Presnell, S.C., and LeCluyse, E.L. (2016). Modeling compound-induced fibrogenesis in vitro using three-dimensional bioprinted human liver tissues. Toxicol. Sci. kfw169.
Olson, H., Betton, G., Robinson, D., Thomas, K., Monro, A., Kolaja, G., Lilly, P., Sanders, J., Sipes, G., Bracken, W., et al. (2000). Concordance of the Toxicity of Pharmaceuticals in Humans and in Animals. Regul. Toxicol. Pharmacol. *32*, 56–67.

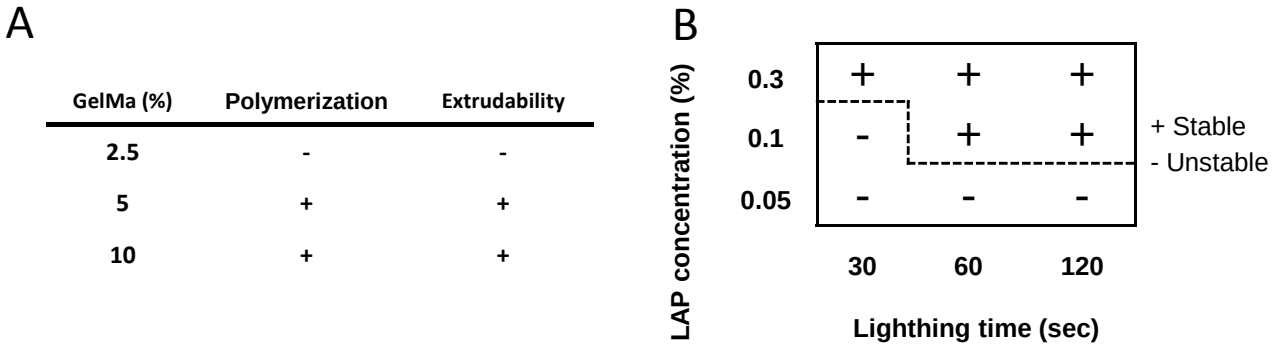
Journal Pre-proof

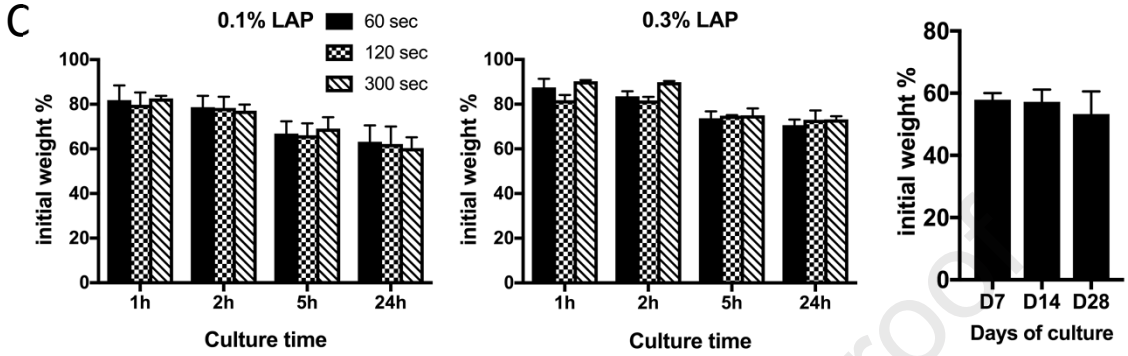
Prestigiacomo, V., Weston, A., Messner, S., Lampart, F., and Suter-Dick, L. (2017). Pro-fibrotic compounds induce stellate cell activation, ECM-remodelling and Nrf2 activation in a human 3D-multicellular model of liver fibrosis. PLOS ONE *12*, 1–17.
Prestigiacomo, V., Weston, A., and Suter-Dick, L. (2020). Rat multicellular 3D liver microtissues to explore TGF-β1 induced effects. J. Pharmacol. Toxicol. Methods *101*, 106650.
Proctor, W.R., Foster, A.J., Vogt, J., Summers, C., Middleton, B., Pilling, M.A., Shienson, D., Kijanska, M., Ströbel, S., Kelm, J.M., et al. (2017). Utility of spherical human liver microtissues for prediction of clinical drug-induced liver injury. Arch. Toxicol. *91*, 2849–2863.
Rebelo, S.P., Costa, R., Estrada, M., Shevchenko, V., Brito, C., and Alves, P.M. (2015). HepaRG microencapsulated spheroids in DMSO-free culture: novel culturing approaches for enhanced xenobiotic and biosynthetic metabolism. Arch. Toxicol. *89*, 1347–1358.
Rouède, D., Schaub, E., Bellanger, J.-J., Ezan, F., Scimeca, J.-C., Baffet, G., and Tiaho, F. (2017). Determination of extracellular matrix collagen fibril architectures and pathological remodeling by polarization dependent second harmonic microscopy. Sci Rep 12197--12197.
Sohara, N., Znoyko, I., Levy, M.T., Trojanowska, M., and Reuben, A. (2002). Reversal of activation of human myofibroblast-like cells by culture on a basement membrane-like substrate. J. Hepatol. *37*, 214–221.
Soumillon, M., Cacchiarelli, D., Semrau, S., van Oudenaarden, A., and Mikkelsen, T.S. (2014). Characterization of directed differentiation by high-throughput single-cell RNA-Seq. BioRxiv 003236.
Stanley, L.A. (2017). Drug Metabolism. In Pharmacognosy, (Elsevier), pp. 527–545.
Théret, N., Musso, O., L'Helgoualc'h, A., and Clément, B. (1997). Activation of matrix metalloproteinase-2 from hepatic stellate cells requires interactions with hepatocytes. Am. J. Pathol. *150*, 51–58.
Troeger, J.S., Mederacke, I., Gwak, G., Dapito, D.H., Mu, X., Hsu, C.C., Pradere, J., Friedman, R.A., and Schwabe, R.F. (2012). Deactivation of Hepatic Stellate Cells During Liver Fibrosis Resolution in Mice. Gastroenterology *143*, 1073-1083.e22.
Van Den Bulcke, A.I., Bogdanov, B., De Rooze, N., Schacht, E.H., Cornelissen, M., and Berghmans, H. (2000). Structural and Rheological Properties of Methacrylamide Modified Gelatin Hydrogels. Biomacromolecules *1*, 31–38.
Vinken, M., Papeleu, P., Snykers, S., De Rop, E., Henkens, T., Chipman, J.K., Rogiers, V., and Vanhaecke, T. (2006). Involvement of Cell Junctions in Hepatocyte Culture Functionality. Crit. Rev. Toxicol. *36*, 299–318.
Wang, X., Yan, Y., Pan, Y., Xiong, Z., Liu, H., Cheng, J., Liu, F., Lin, F., Wu, R., and Zhang, R. (2006). Generation of three-dimensional hepatocyte/gelatin structures with rapid prototyping system. Tissue Eng. *12*, 83–90.
Wang, X., Yan, Y., and Zhang, R. (2007). Rapid prototyping as a tool for manufacturing bioartificial livers. Trends Biotechnol. *25*, 505–513.
Xu, L. (2005). Human hepatic stellate cell lines, LX-1 and LX-2: new tools for analysis of hepatic fibrosis. Gut *54*, 142–151.
Yan, Y., Wang, X., Pan, Y., Liu, H., Cheng, J., Xiong, Z., Lin, F., Wu, R., Zhang, R., and Lu, Q. (2005). Fabrication of viable tissue-engineered constructs with 3D cell-assembly technique. Biomaterials *26*, 5864–5871.
Yang, H., Sun, L., Pang, Y., Hu, D., Xu, H., Mao, S., Peng, W., Wang, Y., Xu, Y., Zheng, Y.-C., et al. (2020). Three-dimensional bioprinted hepatorganoids prolong survival of mice with liver failure. Gut gutjnl-2019-319960.
Zhong, C., Xie, H.-Y., Zhou, L., Xu, X., and Zheng, S.-S. (2016). Human hepatocytes loaded in 3D bioprinting generate mini-liver. Hepatobiliary Pancreat. Dis. Int. *15*, 512–518.

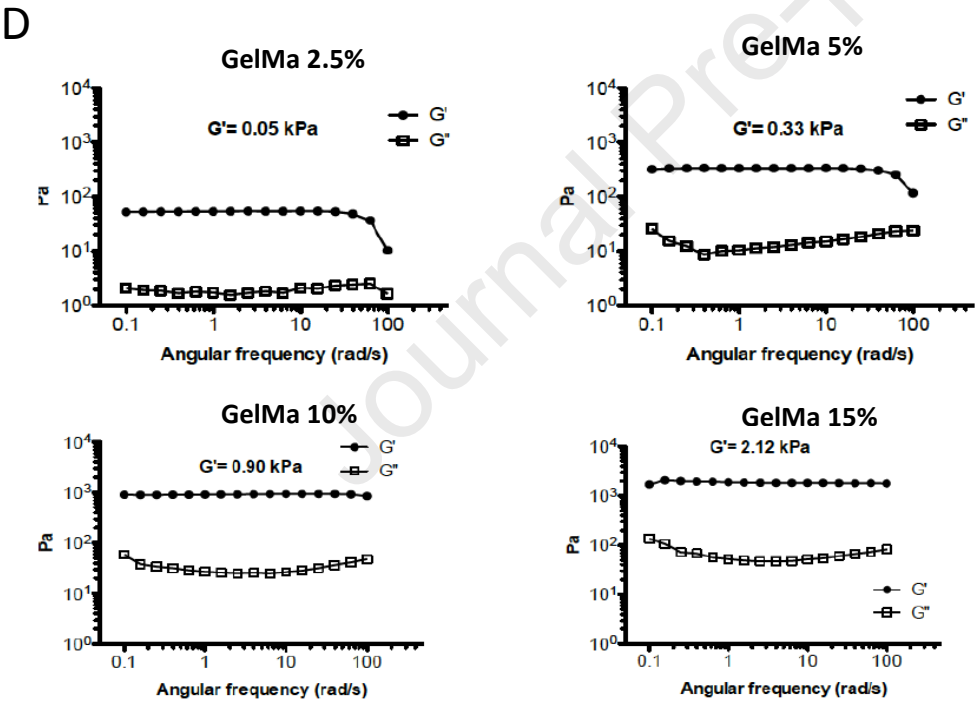
Journal Pre-proof

A

GelMa (%)	Polymerization	Extrudability
2.5	-	-
5	+	+
10	+	+







Journal Pre-proof

Figure 1: Polymerization, printability and physical properties of GelMa.

(A) Polymerization and extrudability at different concentrations: 2.5%, 5% and 10% of GelMa. (B) Structural integrity at 37°C of bioprinted models with 5% GelMa, 1 hour after cross-linking at different LAP concentrations (%) and lighting times (sec). (C) Degradation kinetic of a 5% GelMa structure for 24 hours (left) or 28 days (right) of culture at 37°C after bioprinting and cross-linking, depending on the LAP concentration and lighting duration. Results are presented as mean ± SD of n=3 experiments. (D) Gel stiffness measured by rheology: elastic (G') and viscous (G") modulus of GelMa at different concentrations: 2.5%, 5%, 10% and 15% (w/v).

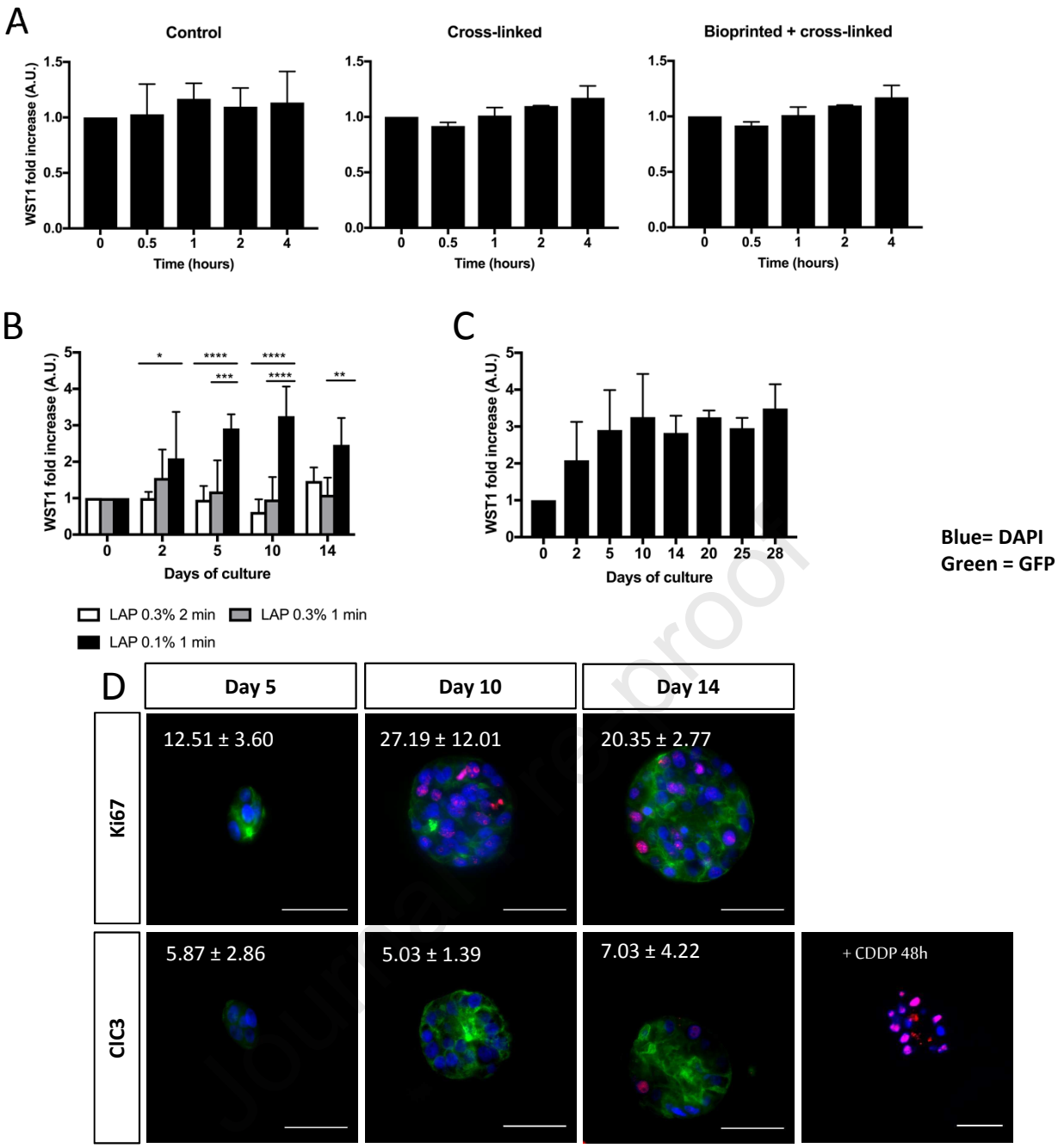
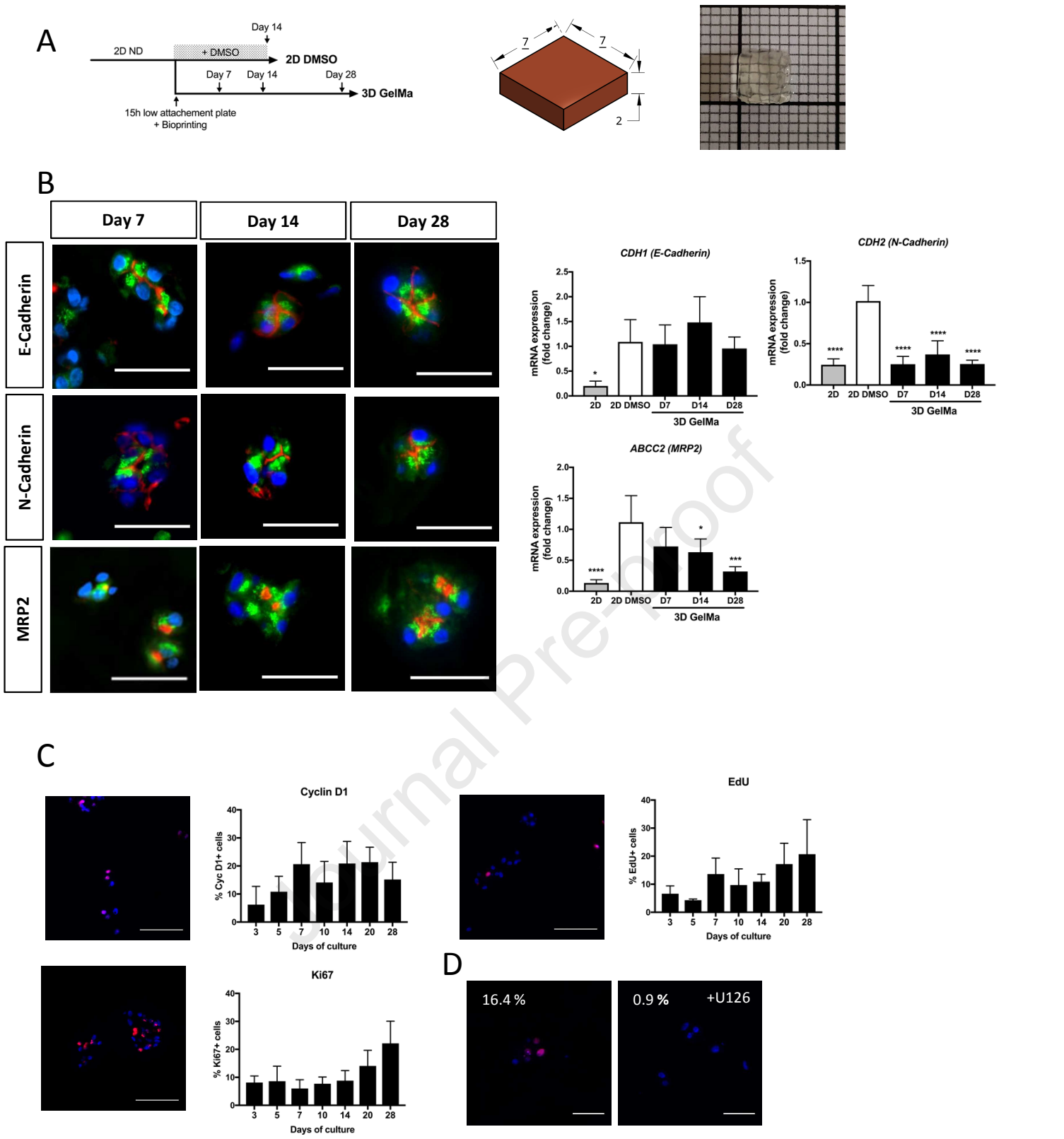


Figure 2: Viability and cluster organization of the Huh7 cells in 5% GelMa.

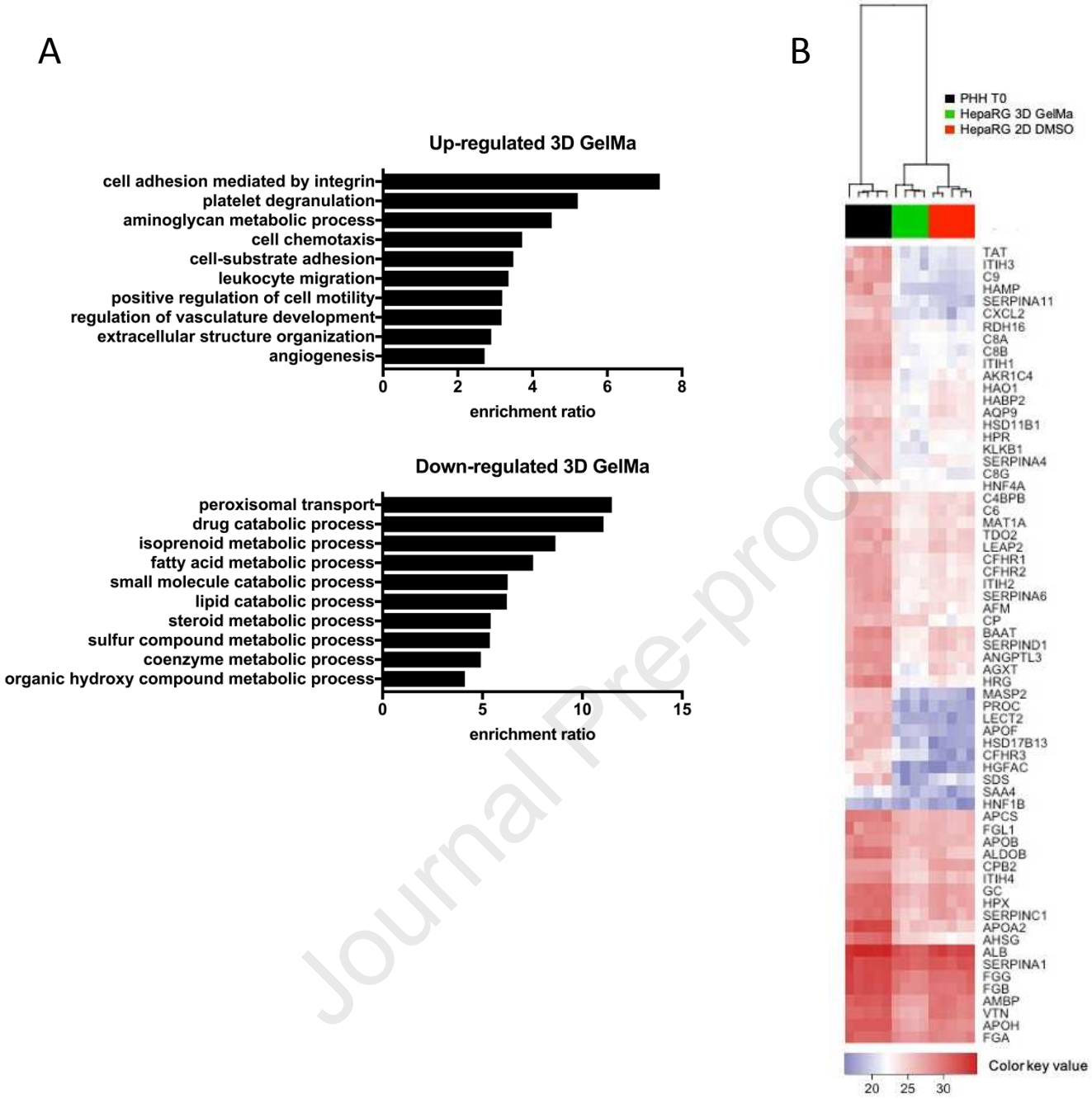
*(A) Short-term viability of Huh7 cells in 5% GelMa, LAP 0.1%, before (control), after 1 min cross-linking, and after bioprinting and 1 min cross-linking at the indicated times (hours) after seeding. (B) Viability of Huh7 cells for 15 days after cross-linking with LAP at 0.1% or 0.3% and after 1 or 2 min cross-linking. (C) Long-term viability of HuH7 cells in 5% GelMa, LAP 0.1%, 1 minKI67 cross-linking, for 30 days of culture. (A-C) Viability data are represented as fold increase of WST1 activities compared to that of control (Day 0). Significance levels: *p ≤ 0.05; **p ≤ 0.01 ; ***p ≤ 0.001; ****p ≤ 0.0001. (D) Cluster organization, proliferation and apoptosis of Huh7-GFP in 5% GelMa at 5, 10 and 14 days after seeding: Blue= DAPI, Green= GFP, Red= Ki67 or cleaved caspase 3 (CIC3). Scale bar = 50 μm. Caspase positive control at day 15 after 20 μM cisplatin treatment for 48 hours (right image); quantifications of the % of Ki67 and cleaved caspase 3 = positive cells/ total nucleus.*

All results are presented as mean ± SD of n=3 experiments.



Journal Pre-proof

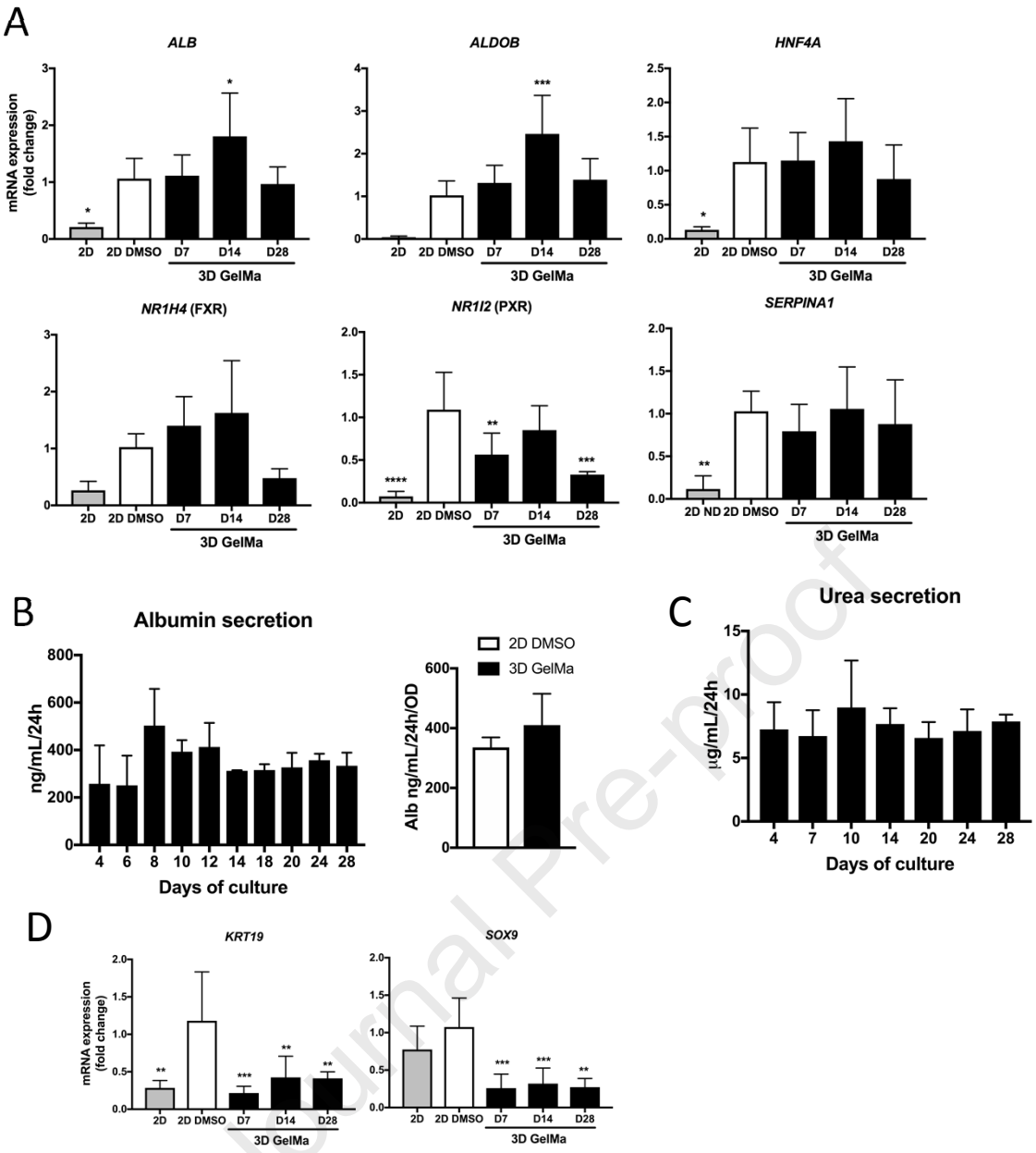
Figure 3: Cluster organization, polarization and proliferation of the HepaRG cells in 5% GelMa.
*(A) Left: Experimental timeline for bioprinted HepaRG (3D GelMa) or 2D DMSO differentiated HepaRG (2D DMSO) Right: CAD design (size in mm) and macroscopic imaging of the printed structure. (B) Immunofluorescence imaging (left) and mRNA expression (right) of E-cadherin (CDH1), N-cadherin (CDH2) and MRP2 (ABCC2) at the indicated times after seeding. Green = albumin, blue = DAPI, Red= E-cadherin or N-cadherin or MRP2. Scale bar = 50 µm. Significance levels of genes expression vs 2D DMSO results: *p ≤ 0.05; ***p ≤ 0.001; ****p ≤ 0.0001.. (C) Staining (left) and quantification (right) of proliferation marker Cyclin D1 and Ki67, and of the incorporation of the thymidine analogue EdU (DNA replication), in 3D HepaRG cells at the indicated times after seeding. Results are expressed as mean ± SD of n=3 experiments. (D) Staining and quantification of EdU incorporation for 48 hours in 3D HepaRG in the absence (left) or presence (right) of U0126 (MEK inhibitor).*



Journal Pre-proof

Figure 4: Transcriptomic analysis of 3D HepaRG

(A) Gene set enrichment analysis based on the functional annotation of the differentially Up and Down-regulated genes in HepaRG cultured for 14 days in 3D in GelMa versus 2D in DMSO. (B) Heatmap (-log2 z-scores) of Ligep genes in freshly isolated human primary hepatocytes (PHH T0, black, 5 samples), HepaRG cultured in 2D with DMSO for 14 days (red, 5 samples) or HepaRG cultured for 14 days in 3D in GelMa (green, 4 samples). Samples and genes are hierarchically clusterd based on Euclidian Distance according to their profile similarity. Elevated (red) and repressed (blue) expression are normalized to the mean of the gene expression.

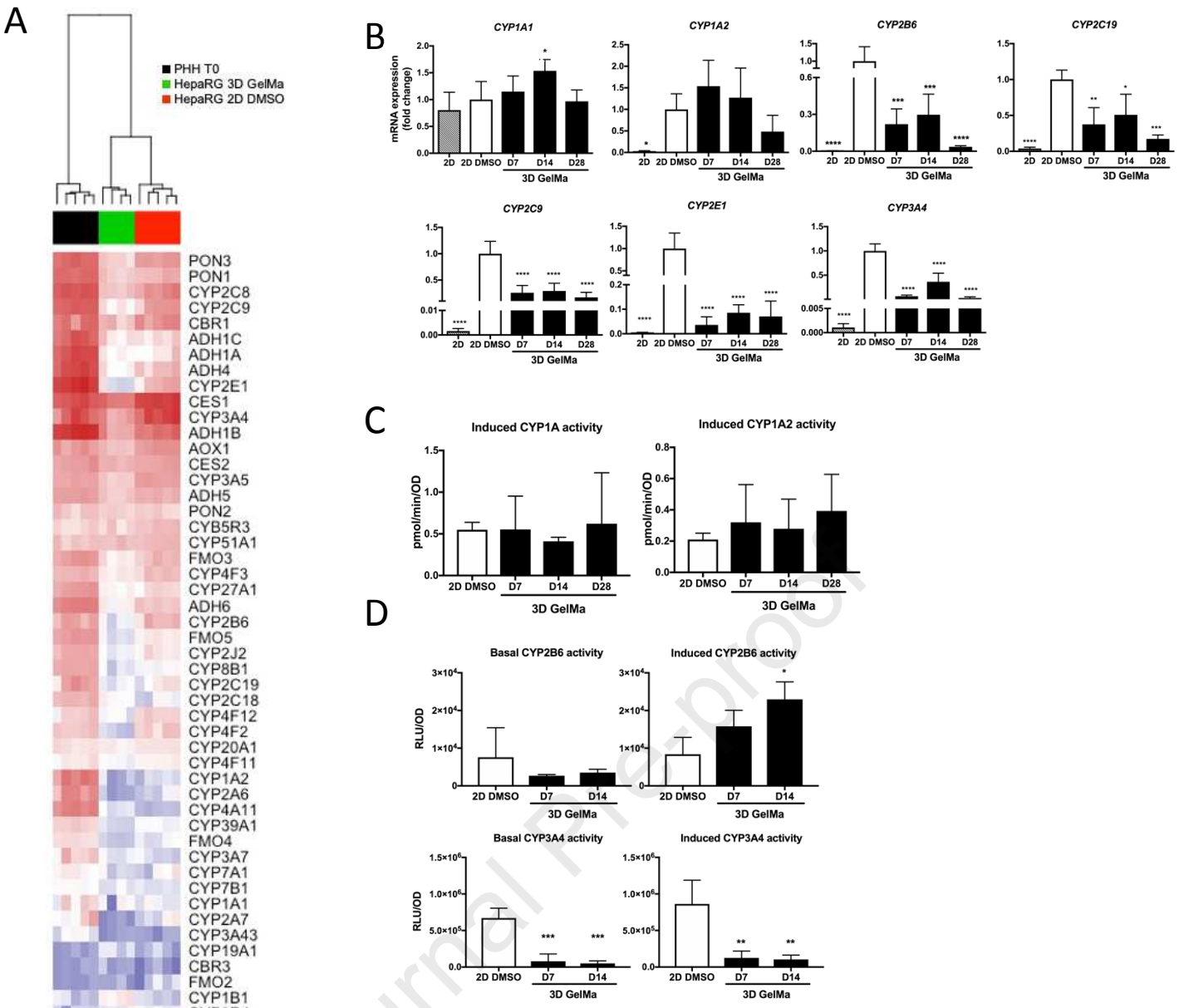


Journal Pre-proof

Figure 5: Hepatic differentiation markers in HepaRG 3D GelMa.

(A) Expression (RT-qPCR) of hepatic differentiation genes in 3D HepaRG (black) at days 7, 14 and 28 of culture, and 2D non differentiated HepaRG (2D), compared to 2D DMSO day 14 (white). (B) Kinetics (left) of albumin secretion by HepaRG 3D GelMa, and comparison (right) to 2D DMSO at day 14 of culture.(C) Urea secretion of HepaRG 3D GelMa over the culture time. (D) HepaRG in GelMa differentiate toward an hepatic rather than a biliary lineage: expressions of SOX9 and KRT19 in 3D GelMa at the indicated times (7, 14, 28 days) and 2D non differentiated HepaRG (2D) were measured by RT-qPCR and compared to 2D DMSO day 14 (white).

*All results are expressed as mean ± SD of n= 3 experiments. Significance levels of genes expression vs 2D DMSO results: *p ≤ 0.05; ** p ≤ 0.01 ; ***p ≤ 0.001.*



E

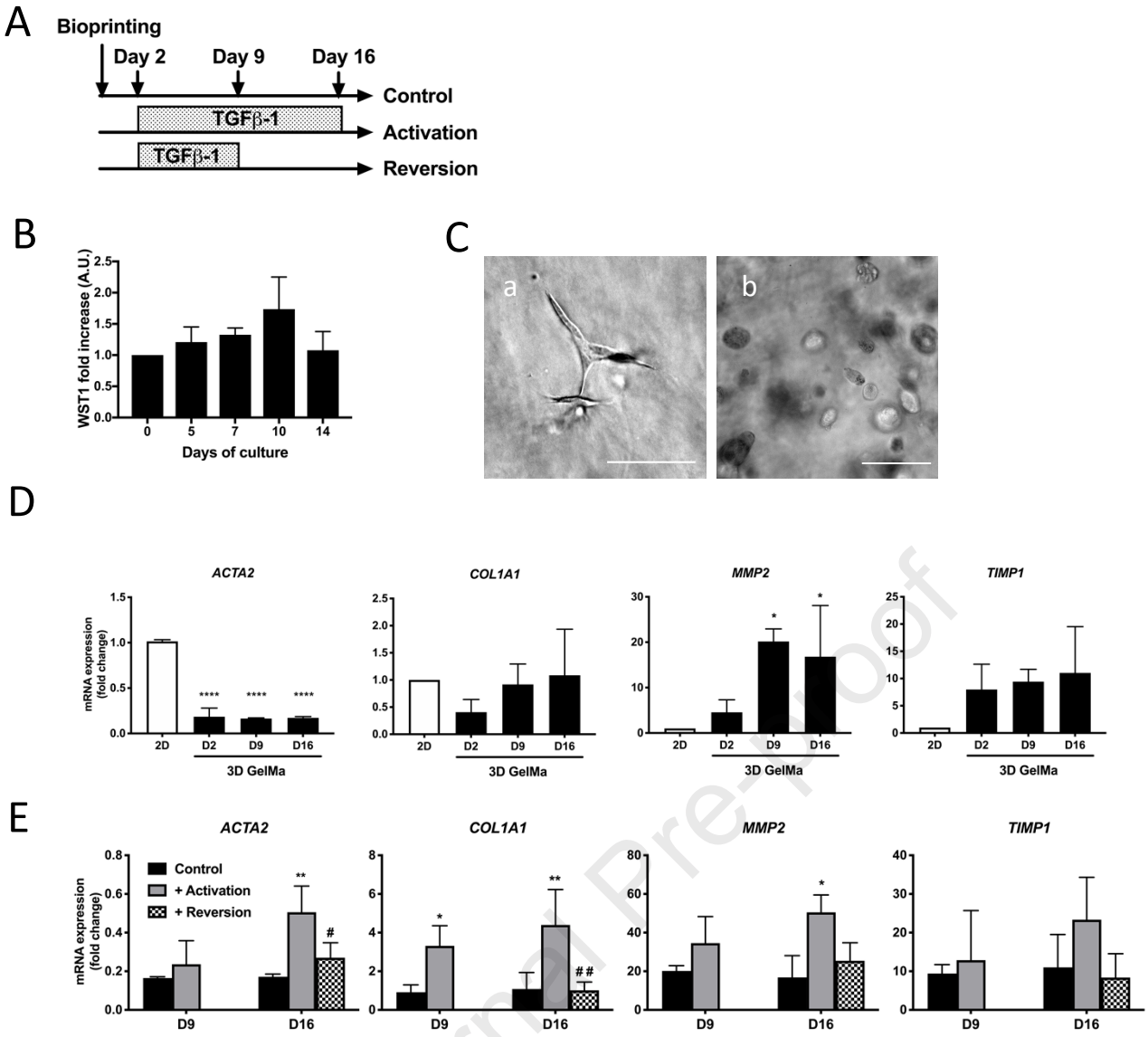
	2D DMSO	3D GelMa D7	3D GelMa D14
CYP1A2	5.04 ± 2.37	14.91 ± 5.72	15.99 ± 5.95
CYP2B6	1.55 ± 0.85	5.85 ± 0.99 **	6.64 ± 1.01 **
CYP3A4	1.26 ± 0.29	1.69 ± 0.55	2.22 ± 0.34 *

Figure 6: Expressions and activities of phase 1 drug-metabolizing enzymes in the HepaRG cells cultured in GelMa.

(A) Heatmap (-log2 z-scores) of phase I enzymes genes in freshly isolated human primary hepatocytes (PHH T0, black, 5 samples), HepaRG cultured in 2D with DMSO for 14 days (red, 5 samples) or HepaRG cultured in 3D in GelMa for 14 days (green, 4 samples). Samples and genes are hierarchically clusterd based on Euclidian Distance according to their profile similarity. Elevated (red) and repressed (blue) expression are normalized to the mean of the gene expression. (B) Quantification of CYPs mRNA expression in 3D GelMa (black) at days 7, 14 and 28 of culture, compared to 2D DMSO at day 14 (white) or 2D undifferentiated HepaRG (2D; grey). (C) CYP1A and 1A2 activities of HepaRG induced by 3MC treatment in 2D DMSO (white) and 3D GelMa (black) was assessed at day 7, 14 or 28 of culture by using the EROD/MROD assay (see M.M). Basal activity not detected. (D) CYP2B6 and 3A4 basal and induced activities in 2D DMSO (white) and 3D GelMa (black) were assessed at day 7 or 14 of culture by using Promega kit (see M.M). (E) Statistical analysis of CYPs induced activities fold increase over basal activities at 7 or 14 days of culture.

*Significance levels of genes expression or activities vs 2D DMSO: *p ≤ 0.05; ** p ≤ 0.01 ; ***p ≤ 0.001; ****p ≤ 0.0001.*

Journal Pre-proof



Journal Pre-Proof

Figure 7 : LX-2 viability, cell morphology and mRNA expressions.

*(A) Experimental timeline for bioprinting and TGFβ-1 mediated activation of LX-2. Structures were bioprinted and LX-2 activation was carried out by treatment with TGFβ-1 (5ng/mL every 48 hours) for 14 days (activation). Alternatively, LX-2 were treated with TGFβ-1 for 7 days, then cultured 7 days without TGFβ-1 (reversion). (B) Viability of LX-2 cells cultured in GelMa 5%, LAP 0,1% for 14 days. Data are represented as fold increase of WST1 activities compared to that of control (Day 0). (C) White light imaging of morphology of LX-2 4 days after seeding in collagen 1 (a) or GelMa 5% (b)(scale bar = 50 µm). (D) Quantification of ACTA2, COL1A1, MMP2 and TIMP1 mRNA expressions in 2D LX-2 at day 4 (white), compared to LX-2 at day 2, 9 and 16 of culture, in 3D GelMa (black). Significatively expressed genes vs 2D LX-2: *p ≤ 0.05; ****p ≤ 0.0001. (E) Quantification of ACTA2, COL1A1, MMP2 and TIMP1 mRNA expressions of LX-2 in GelMa (Control, black), after TGFß-1 mediated activation (grey) and TGFß-1 mediated reversion (squared) at the indicated times. Results were expressed as the n-fold ratios of target gene expression in samples to the mean expression values of the target gene in 2D cultivated LX-2 at D4. Significatively expressed genes vs control (*) or vs activation (#) at day 9 or 16: */# p ≤ 0.05; **/## p ≤ 0.001. All results are expressed as means ± SD of n=3 experiments.*

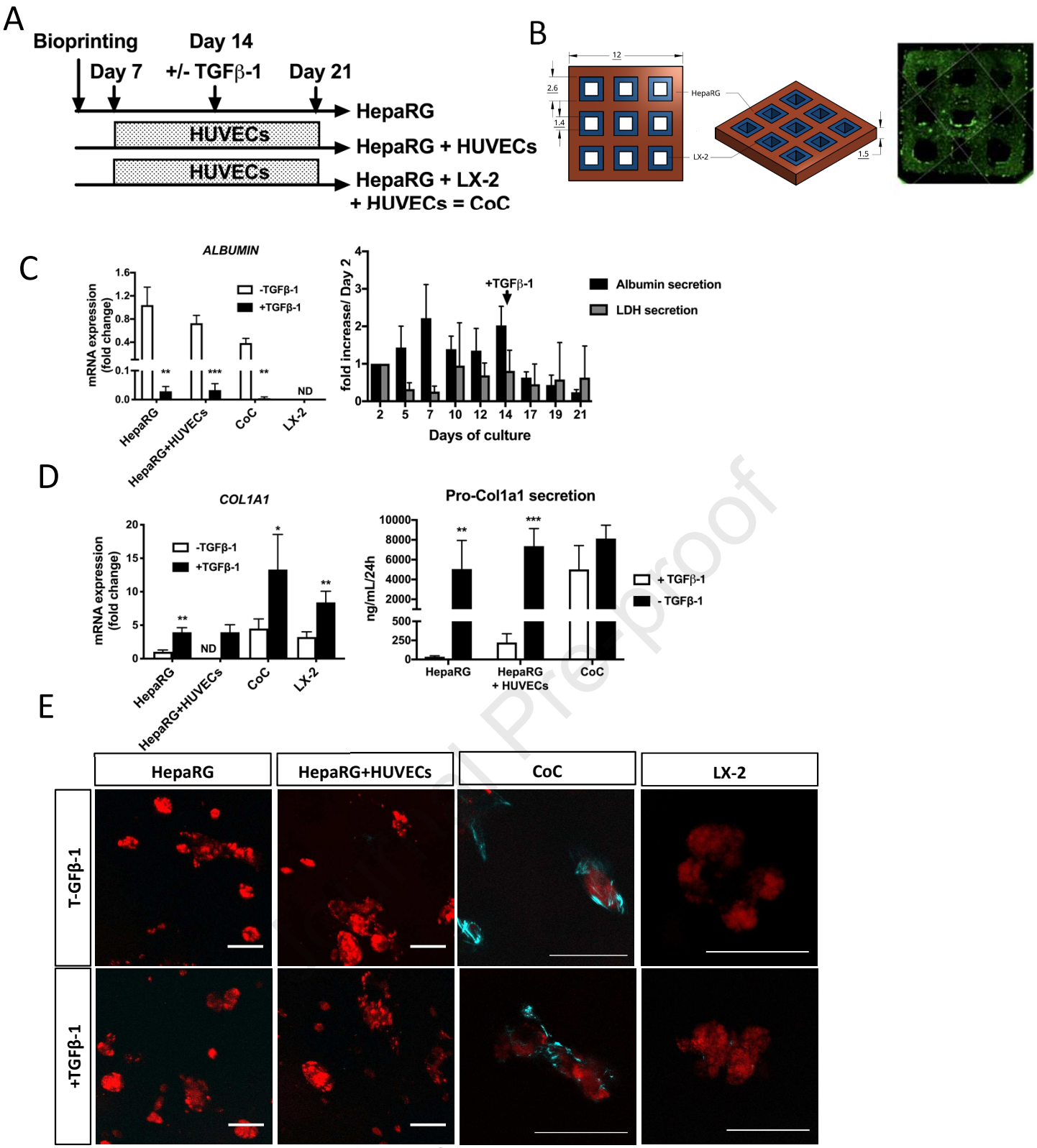


Figure 8: The bioprinted 3D co-culture as a fibrotic model: micro-engineered co-culture made by bioprinting containing HepaRG, LX-2 and HUVEC cells.

*(A) Experimental timeline for bioprinting of HepaRG, HepaRG + LX-2 co-cultures and HUVEC cells seeding. At day 14, cultures were treated or not by TGFβ-1 5ng/mL every 48h for 7 days. (B) Schematic representation of the coculture (CoC) model containing HepaRG (red) and LX-2 cells (blue) bioprinted in GelMa (size in mm). GFP-HUVEC cells have been added at day 7 of culture on the surface of the GelMa (Green, right picture: 4 days after HUVEC seeding). (C) Left: quantification of ALB mRNA expressions without (white) or with (black) TGFß-1 in all 4 conditions. Significatively expressed genes vs HepaRG –TGFβ-1: **p ≤ 0.01; ***p ≤ 0.001. Right: quantification of albumin and LDH secretion of CoC + TGFβ-1 in media, expressed as fold increase of respective level at day 2. (D) Left: quantification of COL1A1 mRNA expressions without (white) or with (black) TGFß-1 in all 4 conditions. Significatively expressed genes vs HepaRG –TGFβ-1: *p ≤ 0.05; **p ≤ 0.01. Right: quantification of procollagen1a1 (Pro-Col1a1) secretion in media at day 2 (grey) and day 21, without (white) or with (black) TGFß-1. Significatively expressed secretion vs D2: ** p ≤ 0.01; ***≤ 0.001. (E) SHG/TPEF imaging of collagen deposition at day 21 (HepaRG, HepaRG+HUVECs, CoC) in all 4 culture conditions. Red = cells (autofluorescence), cyan= collagen 1 fibers (SHG). Scale bar = 50 µm. (HepaRG, HepaRG+HUVECs: 50 µm z-stack of images). All data are expressed as mean ± SD of n=3 experiments.*

Proof

Declaration of interests

☒ The authors declare that they have no known competing financial interests or personal relationships that could have appeared to influence the work reported in this paper.

☐The authors declare the following financial interests/personal relationships which may be considered as potential competing interests:

Journal Pre-proof